60GHz Resonance Isolator

A DISSERTATION
SUBMITTED TO THE FACULTY OF
UNIVERSITY OF MINNESOTA
BY

Qiao Li

IN PARTIAL FULFILLMENT OF THE REQUIREMENTS
FOR THE DEGREE OF
DOCTOR OF PHILOSOPHY

Advisor: Anand Gopinath

December, 2015

Acknowledgement

I would like to give my sincere gratitude to my advisor, Professor Anand Gopinath for his guidance and supports during my Ph.D. study. Professor Gopinath always encourages me when I encounter failures, and point out the direction when I was lost. Many thanks go to the Professors of the committee, Professor Rhonda Frankin, Professor Robert Sainati, and Professor Bernado Cockburn. I also would like to thank my collaborator, Dr. Xiaomei Guo in Boston Technologies Inc, she and her colleagues gave me a lot of support for my project. I am also grateful to all my colleagues Dr. Desalgn Bereka and Vijayaraghavan Panda for the assistance. I would like to thank the staff at the Minnesota Nano Center and Characterization Facility for the great helpful discussions on experimental and data analysis. I also would like to thank the Institute for Rock Magnetism for supporting my experiment. Thanks to Professor Ramesh Hajani and his research group members for their assistance with the tests. Many thanks go to ECE technique support team for their technique support of my research.

Finally, I would like to give my deepest gratitude to my parents for their endless support. I appreciate the patience and encouragement provided by my husband Bo Zhang and my parents. To all of these great people, I am pleased to express my gratitude.

Abstract

Recently, 60GHz system is a hot topic for its large unlicensed bandwidth and small component size. However, some components could not be integrated into the 60GHz communication subsystem either because of their large size or poor performance after integration. One of the most popular ways to build a planar device at high frequency with low cost is to use substrate integrated waveguide (SIW). To make a planar device with low loss at the millimeter waveband, first a 60GHz substrate integrated waveguide with taper transitions from microstrip lines are designed and fabricated. Although planar ferrite isolators based on SIW have been successfully built, all of them work below 20GHz because the ferromagnetic resonance frequency of the traditional ferrite, Yttrium-Iron-Garnet (YIG) is low. Here, to develop a 60GHz isolator based on SIW, a novel C-axis M type Barium thin film ferrite is used. The experimental results proved that the ferromagnetic resonance frequency of this thin film ferrite is much higher than the traditional ferrite materials. In this way a 60GHz H-plane resonance isolator based on SIW is realized with low insert loss and high isolation in the working waveband. Moreover, by integrating a ferromagnetic thin film with ferroelectric thin film, a tunable 60GHz isolator based on SIW was realized. The working frequency of the isolator can be varied with the voltage bias. This method makes it possible to build voltage controlled ferrite devices at 60GHz, which is important for large bandwidth systems.

Table of Contents

List of Tables

List of Figures

CHAPTER 1

INTRODUCTION

1.1 Background and Motivation

High speed and high quality wireless communication is a very hot topic in the recent yeas, the reason is that nowadays wireless devices such as smartphones, tablets and smart hardwares are becoming very popular. Traditional wi-fi systems work at 2.4 GHz and other frequencies to 5.9 GHz. To increase the data rates of the wireless communication system, a large bandwidth is needed [1]. Although ultra-wideband (UWB) technology is proposed to increase the bandwidth [3], it faces strict power limitation at the certain frequency. For example, to avoid interference the Federal Communications Commission (FCC) power spectral density emission limit for UWB transmitters is −41.3 dBm/MHz from 3.1GHz to 10.6GHz [4], which limits the usage of communication system.

Recently, 60GHz is drawing attention because it has a large usable bandwidth. Comparable to UWB, this technology has a comparable bandwidth and less power restrictions [5]. The unlicensed band around 60GHz in different countries are shown in figure 1.1. At least 5GHz continuous bandwidth can be used at 60GHz worldwide [2], which is one of the largest bandwidth in the frequency range.

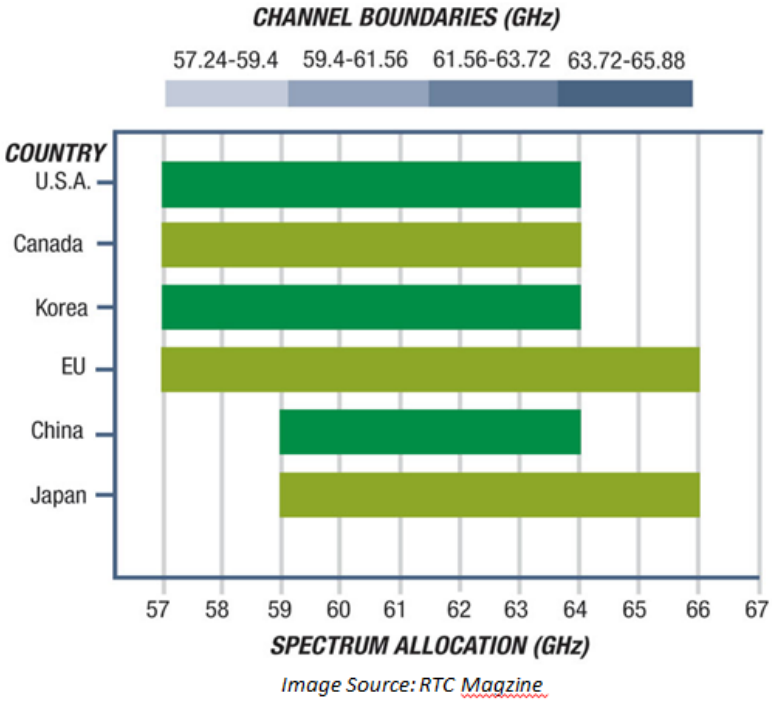

Figure 1.1: Worldwide spectrum availability at the 60 GHz band

Another advantage of using 60GHz system is the high frequency. The high frequency means that the size of the radio-frequency (RF) component is small, and the appearance of Complementary metal–oxide–semiconductor (CMOS) technology makes it possible to produce small size components at high frequency [6], which allows integrating all the RF components into a tiny chip-set. Other benefits of using 60GHz includes inherent security, low interference and high transmit power [7-8].

However, the high frequency also brings challenges. Because of the strong oxygen absorption [9], the power loss at 60GHz is large. This requires the component working at 60GHz must have a high performance especially have a low loss. Besides, for mass-production, the fabrication processes should be low cost [10]. Moreover, some RF

components could not be integrated into the 60GHz system, either because of their large size or poor performance after integration [11].

One of the most promising ways to build a high performance device with low cost at millimeter waveband is using the substrate integrated waveguide (SIW) technology. The SIW structure is first proposed in a patent in 1994 [12]. The SIW combines the traditional metallic waveguide structure and planar technologies. Comparable to the traditional rectangular waveguide, SIW converts the heavy and bulky structure into light and compact planar form. Meanwhile, the metallic waveguide gives SIW a lower loss and a better quality factor than the traditional planar stuctures [13]. Moreover, the existing fabrication technologies such as standard printed circuit board (PCB) [14] and low-temperature co-fired ceramic (LTCC) [15] make SIW to be low cost and highly reliable. Recently many components have been built using SIW technology, including filters, antennas and receivers [16-18]. Moreover, several system-on-substrate integrations are realized using SIW [19-20]. SIW not only makes it possible to fabricate the low cost 60GHz components with high performance, but also helps solve the tiny chip-set integration problem.

Ferrite devices are used many in communication systems including phase shifters, filters, isolators and switches. Among all the ferrite components for 60GHz system, the isolator is the one of the most desired one. The ideal isolator is a two-port device which makes the transmission only occurs in one direction [21]; it is widely used in radio frequency (RF) systems as the duplexer, multiplexers, and signals generate/transmit protections. Although some isolators have been developed using SIW technologies [22-

24], most of them are below 20 GHz. The reason is that the performance of the isolator relies on the magnetic material, and most of the isolators use yttrium iron garnet (YIG) ferrites. However, the ferromagnetic resonance frequency (FMR) of YIG is only around 4GHz [25]. The common way to increase the working frequency of the isolator is using a large magnetic bias. In most of the cases electromagnets are employed because of the low FMR of ferrite material [26-27]. But the electromagnet is bulky and expensive, which is not suitable for planar devices. To make small size 60GHz ferrite devices, a new M-type Barium ferrite (BaM, $BaFe_{12}O_{19}$) is considered to be the future of high frequency ferrite devices. Previous reports prove that the FMR of BaM ferrite is around 60GHz [28], which makes it possible to make ferrite devices working at high frequency with low cost.

Meanwhile, the 60GHz communication system is a wide bandwidth system, and the wide bandwidth communication system has a great need of frequency tunable components especially for voltage biased tunable isolators. However, the traditional isolator could not satisfy the requirements because the working frequency depends on the ferromagnetic resonance (FMR) of ferrite material in the device, and usually the FMR of the certain ferrite material is fixed. To solve this problem, many tunable isolators have been designed. Some of them use the matching circuit to change the working frequency [29], which is complex. Some papers design a ferrite device structure in the waveguide to tune the center frequency [30-31], but the device needs a bias magnetic field. Without the changing of the ferrite material, it is unlikely to realize a voltage biased tunable isolator. By combing the ferromagnetic material and a ferroelectric material together, one can get a multiferroic heterostructure. Reports demonstrate that the FMR of the multiferroic

heterostructures can be modified by varying the electric filed [32-33]. The reason is that the dielectric constant of the layers changes with the bias voltage [34]. The appearance of multiferroic heterostructure makes it possible to build a tunable ferrite device.

1.2 Research Objectives

The main objective is to build a planar isolator working at 60GHz. The SIW is used as the waveguide because it can be built on a thin substrate. To make the device work functionally at 60GHz, the SIW is expected to have a low insertion loss at the working band. Besides, the key to making the isolator work is to use a BaM thin film with a high FMR frequency than the tranditional ferrite material. To achieve this goal, the thin film ferrite should have the minimum defects after the coating. Another difficulty of building a planar isolator at high frequency is that the loss increases with the distance. To solve this problem, the BaM thin film should be put at the optimized position so that the isolation is the largest and the device length is the smallest. In this way, by using the SIW structure together with an optimized BaM thin film strip, the 60GHz planar isolator can be made. The planar isolator is expected to have an isolation larger than -10dB at the working frequency without a magnetic bias or only with a small magnetic bias.

Furthermore, based on the 60GHz planar isolator structure, an electric fieled tunable isolator can be realized. Since it is possible to get a FMR response at 60GHz with a small magnetic bias using a BaM ferrite thin film, if the BaM ferrite thin film is combined with a ferroelectric material, it is possible to make a multiferroic heterostructure with the electric tunability at 60GHz. Reports have found that the FMR response of Barium/Platinum/Barium Strontium Titanate (BaM/Pt/BST) heterostructure shows an

electric tunability at millimeter wave frequencies [35-37]. So using the BaM/Pt/BST heterostructure can help make a tunable ferrite device working at a high frequency even with a small magnetic bias. Besides, with the SIW structure, the ferrite device will be small and fit in a tiny chip-set. The tunable isolator is expected to have a low loss as well as a high isolation in the working band other than electric tunability.

1.3 Thesis Overview

First the structure of SIW is introduced in chapter 2. The simulation results on 60GHz SIW with microstrip lines and taper transitions are given, and different SIW structures are compared. Then the fabrication process of building a SIW on alumina substrate with Platinum coating is presented, and a test platform for 60GHz measurement is designed. The measurement results are discussed later and compared with the simulation results.

In chapter 3, a 60GHz planar isolator based on SIW structure is presented. The principle of self-biased thin film ferrite is introduced, and different kinds of ferrite isolators are compared. Two kinds of 60GHz H-plane resonance isolator based on SIW structure are designed and fabricated, one has single-side ferrite strip and the other one has double-side ferrite strip. The performance of these two isolators is measured using the 60GHz test platform and compared.

Chapter 4 discusses the 60GHz tunable isolator based on SIW structure. The electric tuning property of multiferroic films heterostructure is introduced. A 60GHz voltage biased tunable isolator is built using this kind of heterostructure. And the tunability of the device at 60GHz is presented.

Finally, the conclusions are given and the future work suggested for 60GHz microstrip line isolator is discussed in chapter 5.

CHAPTER 2

THE 60GHZ SUBSTRATE INTEGRATED WAVEGUIDE

2.1 Substrate Integrated Waveguide

A substrate integrated waveguide (SIW) is a dielectric substrate with conducting layers on top and bottom surfaces, and the conducting layers are connected by two rows of metalized cylindrical holes which function as the wall of the waveguide [13]. The structure is shown in figure 2.1.

The SIW combines the traditional metallic waveguide structure and planar technologies together. Compared to the traditional rectangular waveguide, SIW converts the heavy and bulky structure into light and compact planar form. Besides, the metallic waveguide properties make SIW has lower loss and better quality factor compared to the lossy planar structure [38].

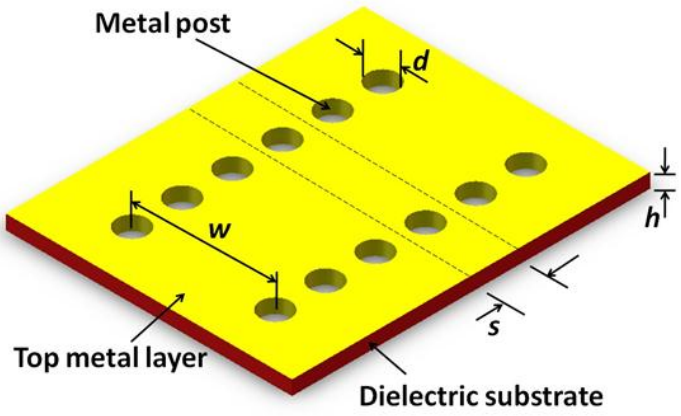

Figure 2.1: The geometry of SIW

The wave propagation in SIW is similar to the traditional rectangular waveguide. For TEm0 mode wave, the surface current flows vertically along the top and bottom metal surfaces. When the gap between the posts is small, the metal posts function as the wall of the rectangular waveguide [39]. So the radiation microwave signal power is retained inside the SIW and there will be no leakage. But this rule doesn't fit the other modes due to the specific geometry property of SIW, when the surface current is not vertical on the side walls [13].

Sometimes people use the equivalent rectangular waveguide model is used to analyze the wave propagation in the SIW, and the equivalent width is [40]:

$$w_{eff} = w - \frac{d^2}{0.95s} \tag{2.1}$$

Here, Weff is the width of the equivalent rectangular waveguide, d is the diameter of the metal posts and s is the space between the posts.

A more accurate method is to use full wave electromagnetic model [41]. This method first considered the unit cell of the SIW and then applies it to the periodic structure. Different approaches have been used to solve the full wave model, such as finite-difference time domain (FDTD) method [42], boundary integral-resonant mode expansion (BI-RME) method [43], integral equations [44] and surface impedance concept [45].

Based on the SIW models, the design rules of SIW can be obtained by considering the loss, the leakage as well as the band gap. Here the band gap effect is caused by the periodic post structure of SIW [47].

Due to the similarity between rectangular waveguide and SIW, the width w is decided by the cutoff frequency fc of the waveguide. For TE10 mode, the cutoff frequency $(f_c)_{10}$ can be got by the following equation [48]:

$$(f_c)_{10} = \frac{1}{2\pi\sqrt{\mu\varepsilon}}\sqrt{(\frac{\pi}{w})^2} \tag{2.2}$$

The other dimensions of SIW are decided by the following rules [49]:

$$s > d \tag{2.3}$$

$$\frac{s}{\lambda_c} < 0.25 \tag{2.4}$$

$$\frac{s}{d} < 2 \tag{2.5}$$

$$s > \lambda_c/20 \tag{2.6}$$

The first equation is to avoid the metal posts intersection. The second equation is to avoid the band gap effect. The third equation is to minimize the radiation leakage, and the last equation is to avoid over-perforated substrate [50].

The operation frequency of the SIW is determined by the following three dimensions: the width of the waveguide w, the diameter of the posts d and the space between the posts s. Moreover, the thickness h plays no role in the wave propagation [51], which makes it perfect for planar device.

2.2 Different SIW Structures at 60GHz

Based on the different post shapes and substrate layers, the SIW may be separated into several groups: the half-mode SIW [52-55], the substrate integrated fold waveguide [56-59], substrate integrated slab waveguide [60-63] and substrate integrated ridge

waveguide [64-68]. Some of these SIWs can reduce the substrate size, and some of them aim to reduce the cut off frequency. In our project, since the working frequency is 60GHz, the component size is already small. So only the traditional SIW will be considered.

Since the device is working at high frequency, alumina substrate is used in this case. SIW on alumina substrate is designed and simulated in Ansoft HFSS program (Ansoft Inc.).

2.2.1 SIW with Single-layer Posts

The first kind of the SIW is with single-layer posts. According to the calculation, the maximum parameters that can be used on alumina substrate are d=0.37mm, s=0.74mm, and w=1.48mm. Considering the machining tolerance (0.02mm), d=0.35mm design is used on alumina substrate instead of d=0.37mm. The geometry of SIW of the alumina substrate is shown in figure 2.2. The result of the simulation is plotted in the graph of propagation constant β against frequency and is shown in figure 2.3. Figure 2.4 is the simulation result on reflection coefficient (S_{11}) and transmission coefficient (S_{21}) in a 50 Ohm system. The results of figure 2.3 and figure 2.4 imply that at 60GHz signal can be propagated through the SIW on alumina substrate.

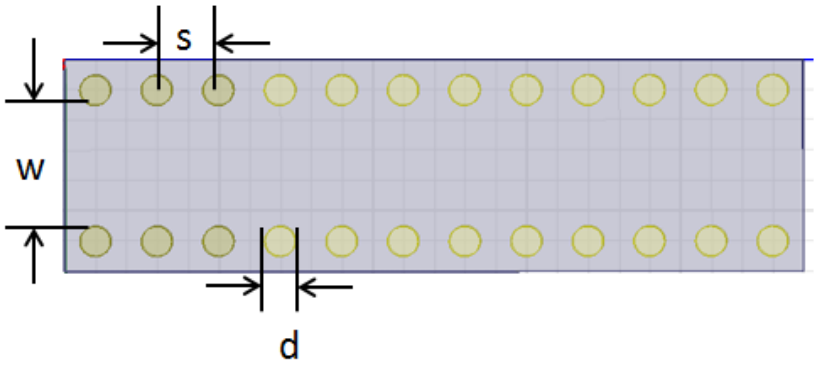

Figure 2.2: Geometry of SIW with single-layer posts

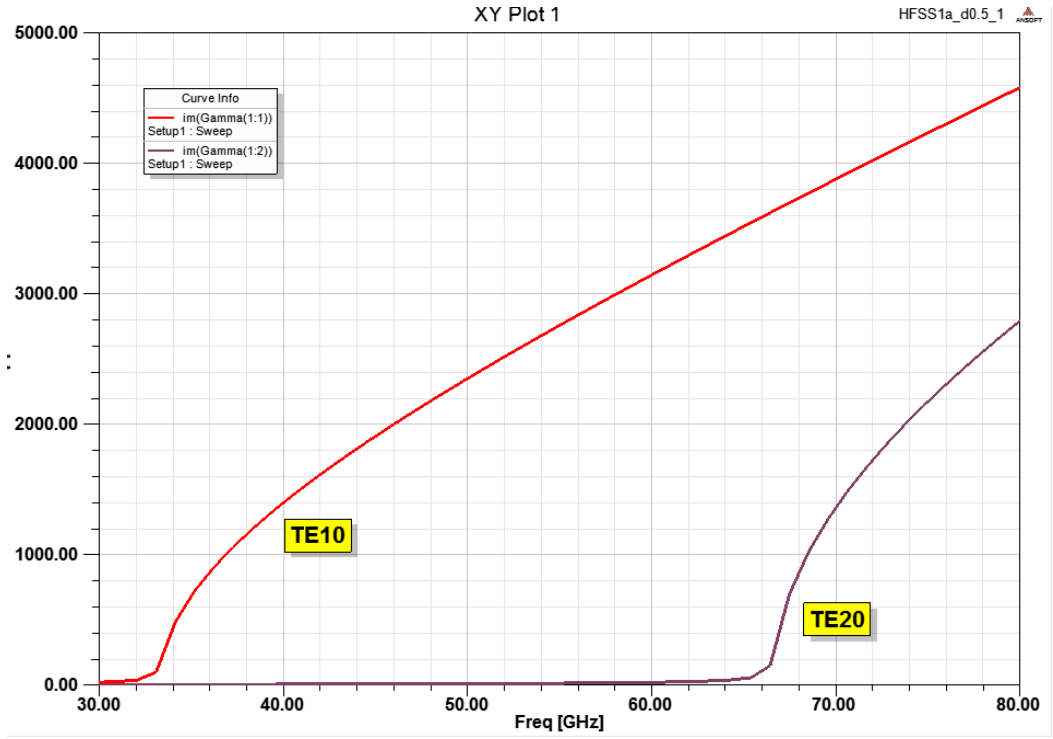

Figure 2.3: Propagation Constant TE_{m0} vs frequency (SIW with single-layer posts)

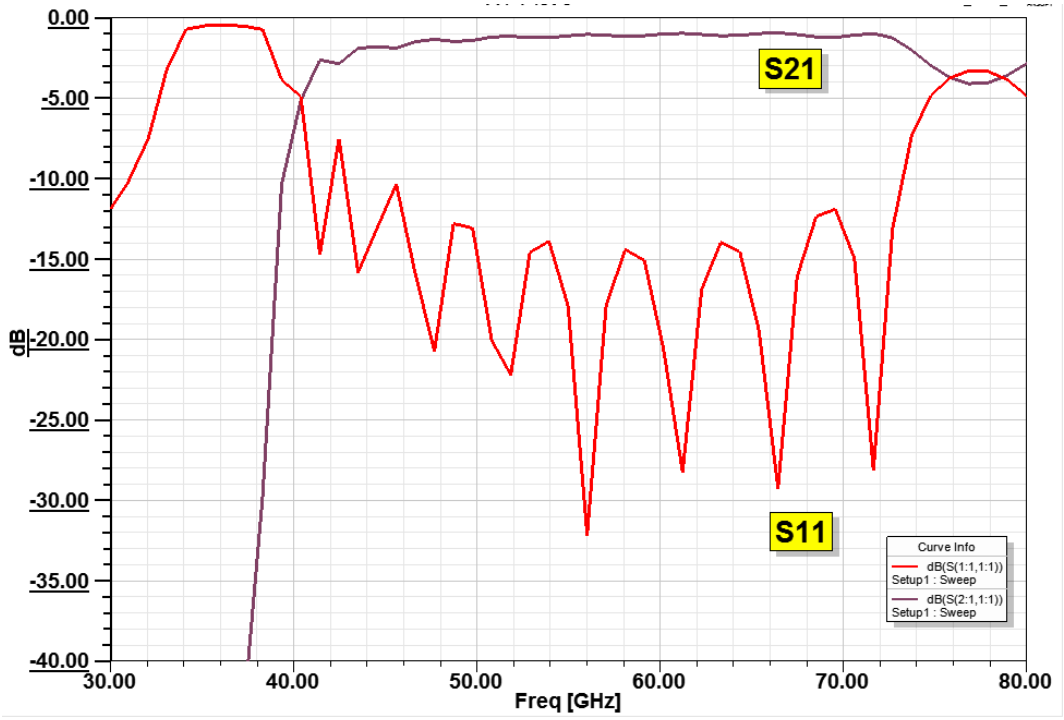

Figure 2.4: S_{11} and S_{21} vs frequency (SIW with single-layer posts)

2.2.2 SIW with Double-layer Posts

However, to decrease the attenuation constant (α) at 60 GHz, a large SIW surface area is needed. So figure 2.2 needs to be improved to get a larger surface area. SIW with double-layer posts is designed to increase w. The geometry of is shown in figure 2.5, the parameters are d=0.25mm, s=0.5mm, and the maximum w is increased to 1.8mm. The result of the simulation is plotted in graph of propagation constant against frequency and is shown in figure 2.6. The result in figure 2.6 is almost the same as figure 2.3, which means the SIW with double-layer posts can work as well as SIW with single-layer posts. Nevertheless, according to Pozar's book [69], figure 2.7 will give a smaller attenuation constant (α) compared with figure 2.4.

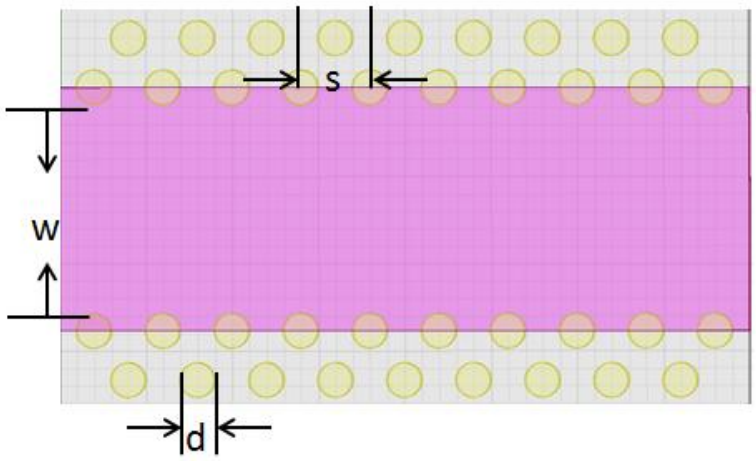

Figure 2.5: Geometry of SIW with double-layer posts

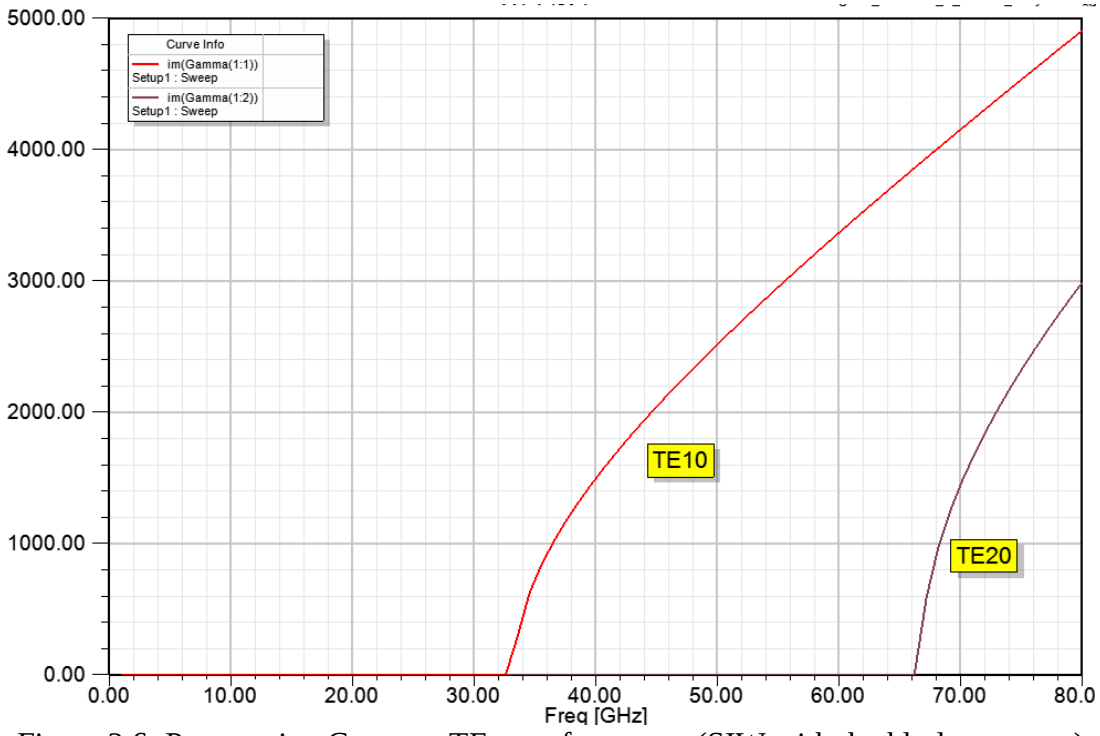

Figure 2.6: Propagation Constant TE_{m0} vs frequency (SIW with double-layer posts)

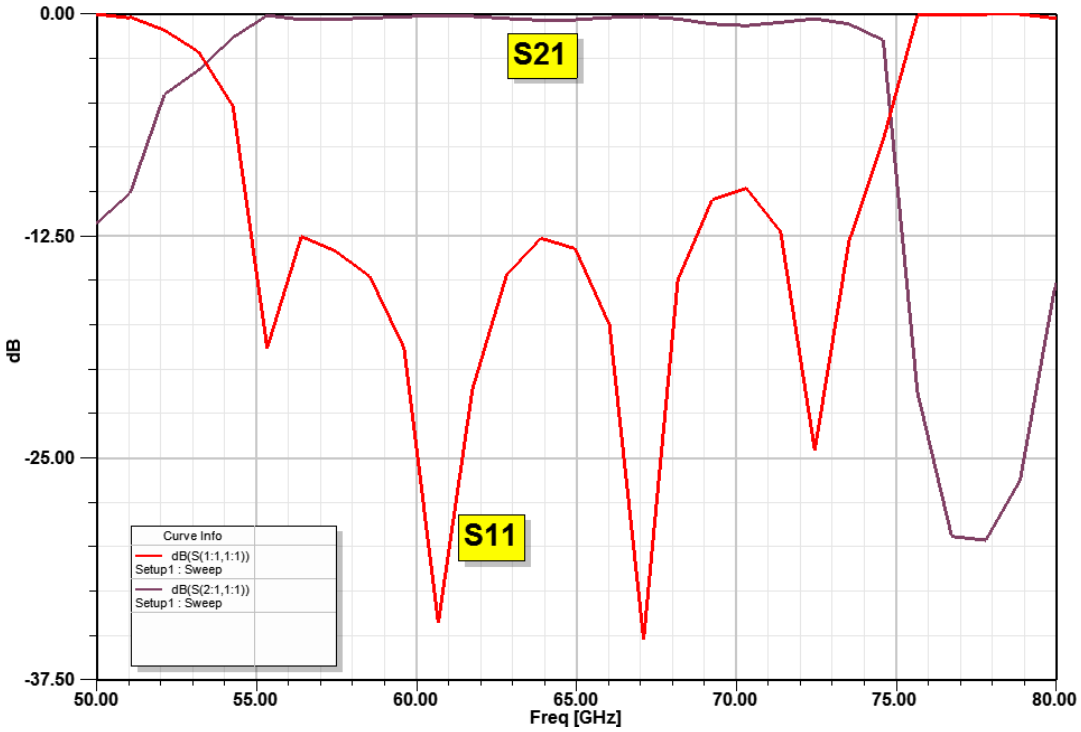

Figure 2.7: S_{11} and S_{21} vs frequency (SIW with double-layer posts)

However, laser processing technology needs to be used for drilling holes on alumina substrates. By consulting with the laser processing company, the space of SIW with double-layer posts is too small (s=0.5mm), and the substrate will be likely to crack during the fabrication. As a result, SIW with single-layer posts is used in the project.

2.3 Microstrip Lines and Taper Transitions

During the test, the SIW must be connected to the other connectors or equipment. The microstrip line is widely used in the microwave applications for its small size and ease of integration. As a result, a microstrip line is needed to connect the SIW with the connectors. Besides, to reduce the loss from microstrip line to the SIW, a taper transition between these two transmission lines is employed.

2.3.1 60GHz Microstrip Lines

Since the connectors need to be soldered on the microstrip lines, if the line parameters are too small it will be difficult to solder. Although the thickness of the substrate has no influence on the SIW, the thickness of the substrate does affect the dimensions of the microstrip lines. Through the calculation of microstrip lines, it is found that with the decreasing of substrate thickness both the line width and taper width will decrease. So initially, it is assumed that a thicker substrate should be used.

As a result, 0.5mm thick alumina substrate was first proposed for the SIW and the microstrip line. The microstrip line length is l_{ms}=0.82mm and line width is w_{ms}=0.7mm. However, the simulation result in figure 2.8 shows that in this case, the cutoff frequency of TE_{20} drops to 33GHz, and at 60GHz both TE_{10} and TE_{20} exist. The change of cut off frequency on the first higher mode is caused by the substrate thickness.

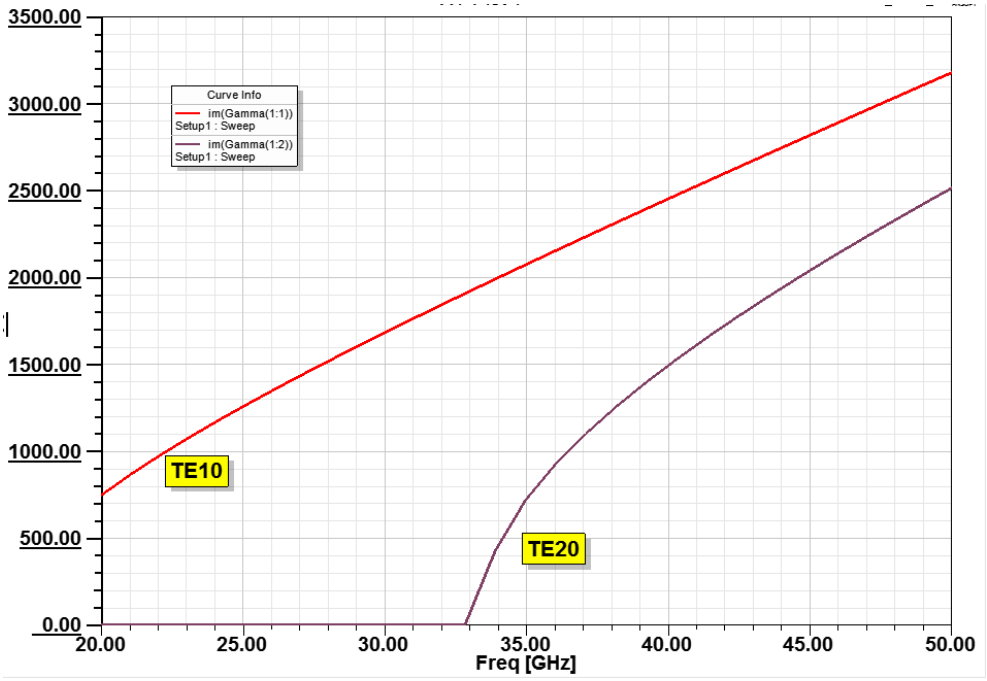

Figure 2.8: Propagation Constant TE_{m0} vs frequency (0.5mm thick alumina SIW with microstrip line)

The cut off frequency of first higher mode is [13]:

$$f_c = \frac{300}{\sqrt{\varepsilon_r}(2w+0.8h)} \tag{2.7}$$

The frequency where significant coupling occurs between the quasi-TEM mode, which is the first microstrip mode and the lowest order surface wave mode is given by [13]:

$$f_T = \frac{150}{\pi h}\sqrt{\frac{2}{\varepsilon_r - 1}}\tan^{-1}(\varepsilon_r) \tag{2.8}$$

And the cut off frequency of first higher mode is [13]:

$$f_c = \frac{300}{\sqrt{\varepsilon_r}(2w+0.8h)} \tag{2.9}$$

Here, f_c is the cut off frequency of the first higher mode and f_T is the frequency where the coupling occurs.

To meet the requirement of the working frequency, 60GHz for this project, should be smaller than both f_T and f_c. Since f_T is smaller than f_c, assume that f_T=60GHz, it is found that the minimum substrate thickness for both alumina (ε_r=9.6) is around 0.5mm. Considering the thickness of metal coating on the substrate and substrate roughness, at 60GHz the substrate thickness should be less than 0.5mm, to make sure that the microstrip has only the fundamental mode. As a result, the thickness of the alumina substrate is set to be h=0.25mm.

The dimensions of the 1.85mm connectors also affect the dimensions of the microstrip line. It is found that the microstrip connector is about 2mm long. As a result, the microstrip line should at least 2.5mm to launch the microstrip connector. However, if the length is too long, the insertion loss will be increased. So the length of the microstrip line is set to be 2.8mm and the corresponding width of the microstrip line is 0.3mm.

2.3.2 The Design of Taper Transitions

To connect SIW with microstrip and reduce the discontinuity effects, a taper transition is designed. The taper transition connects the conductor of the microstrip lines to the top surface of the SIW, while the ground planes of the two components are also connected together. The transitions can make full wave transitions without optimization [70]. To get the optimum width w_{taper} of taper transition, the microstrip line is modeled equivalent TEM waveguide with a width of w_e. The following equations are used to calculate w_e:

$$\frac{1}{w_e} = \begin{Bmatrix} \frac{60}{\eta h}\ln\left(8\frac{h}{w_{taper}} + 0.25\frac{w_{taper}}{h}\right) \\ \frac{120\pi}{\eta h\left[w_{taper}/h + 1.393 + 0.667\ln\left(w_{taper}/h + 1.444\right)\right]} \end{Bmatrix} \tag{2.10}$$

Here, η is the intrinsic impedance and h is the substrate thickness. The first part of the equation is used when w_{taper}/h is smaller than 1 and the second part is used when w_{taper}/h is larger than 1. And w_e can also be obtained by this equation:

$$\frac{1}{w_e} = \frac{4.38}{a_e} e^{-0.627\frac{\varepsilon_r}{\frac{\epsilon_r+1}{2}+\frac{\varepsilon_r-1}{2}*\frac{1}{\sqrt{1+12h/w_{taper}}}}} \tag{2.11}$$

Using equation 2.10 and equation 2.11, the optimum width w_{taper} of the taper transition can be solved.

Taper length should be chosen as a multiple of quarter wavelength [71]. According to these equations, for w=1.4mm SIW, a_e is about 1.2mm, w_{taper}=1.8216*h mm, l_{taper}=0.58*n mm (n=1, 2, 3…). Figure 2.9 shows the microstrip and taper transition on SIW.

Figure 2.9: Microstrip line and taper transition on SIW

2.3.3 Comparison of Different Taper Lengths

The different taper length will give a different insertion loss. To minimize the insertion loss at 60GHz, five taper lengths are tested: λ/4, λ/2, 3λ/4, 5λ/4 and 7λ/4. The simulation results on reflection coefficient (S11) and transmission coefficient (S21) at different taper lengths are shown in figure 2.10.

Simulation results show that with the taper length increase, S11 is decreasing. And when taper length is 5λ/4 and 7λ/4, the results are almost the same as 3λ/4. So the taper dimensions are: l_{taper}=3λ/4=1.74mm and w_{taper}=0.6mm.

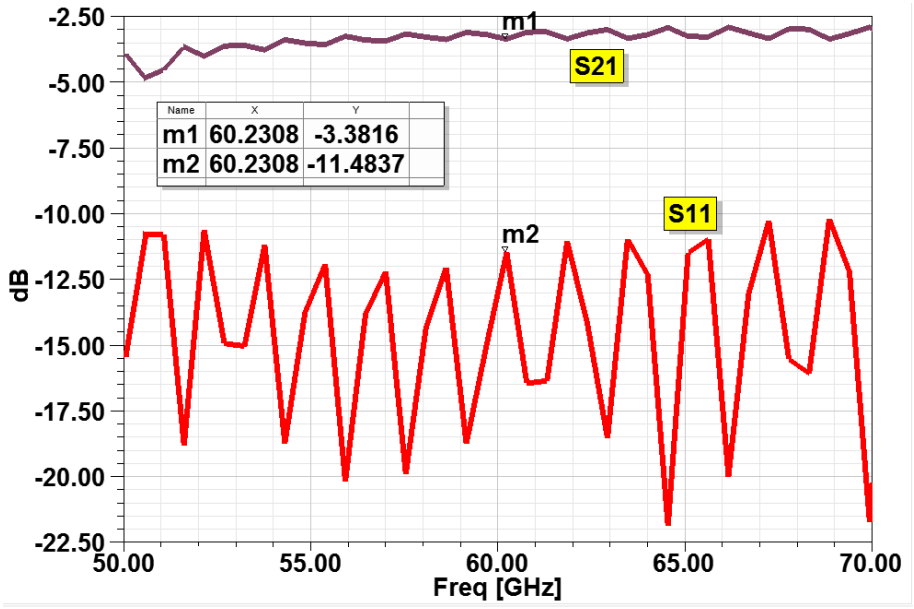
m1
S21
Name X Y
m1 60.2308 -3.3816
m2 60.2308 -11.4837
S11
m2
dB
-2.50
-5.00
-7.50
-10.00
-12.50
-15.00
-17.50
-20.00
-22.50
50.00
55.00
60.00
65.00
70.00
Freq [GHz]

(a)

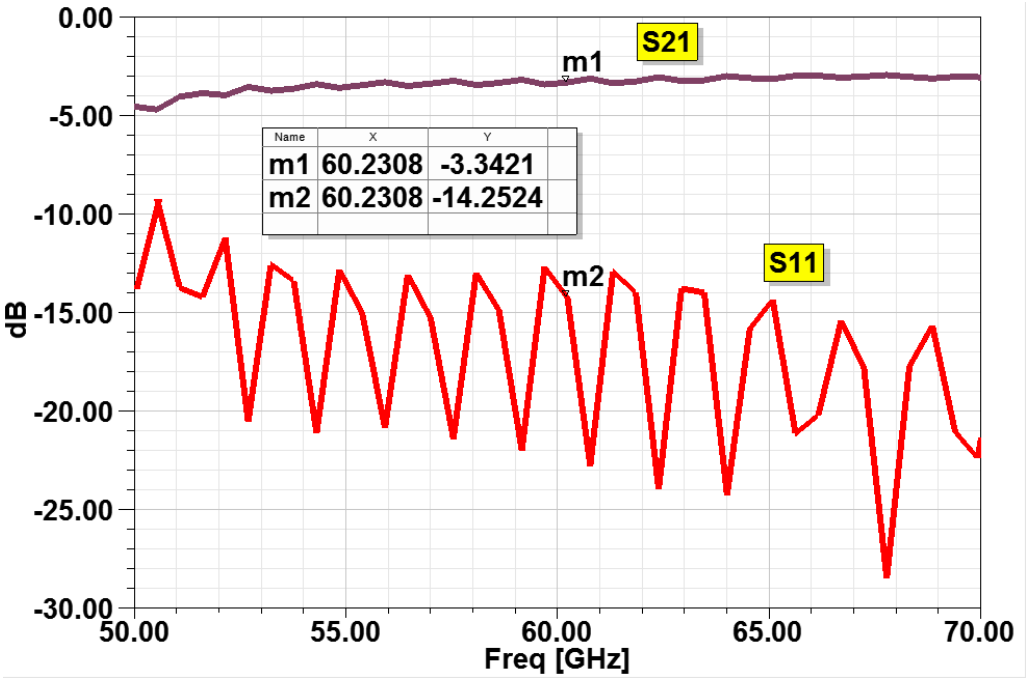
S21
m1
Name X Y
m1 60.2308 -3.3421
m2 60.2308 -14.2524
S11
m2
dB
0.00
-5.00
-10.00
-15.00
-20.00
-25.00
-30.00
50.00
55.00
60.00
65.00
70.00
Freq [GHz]

(b)

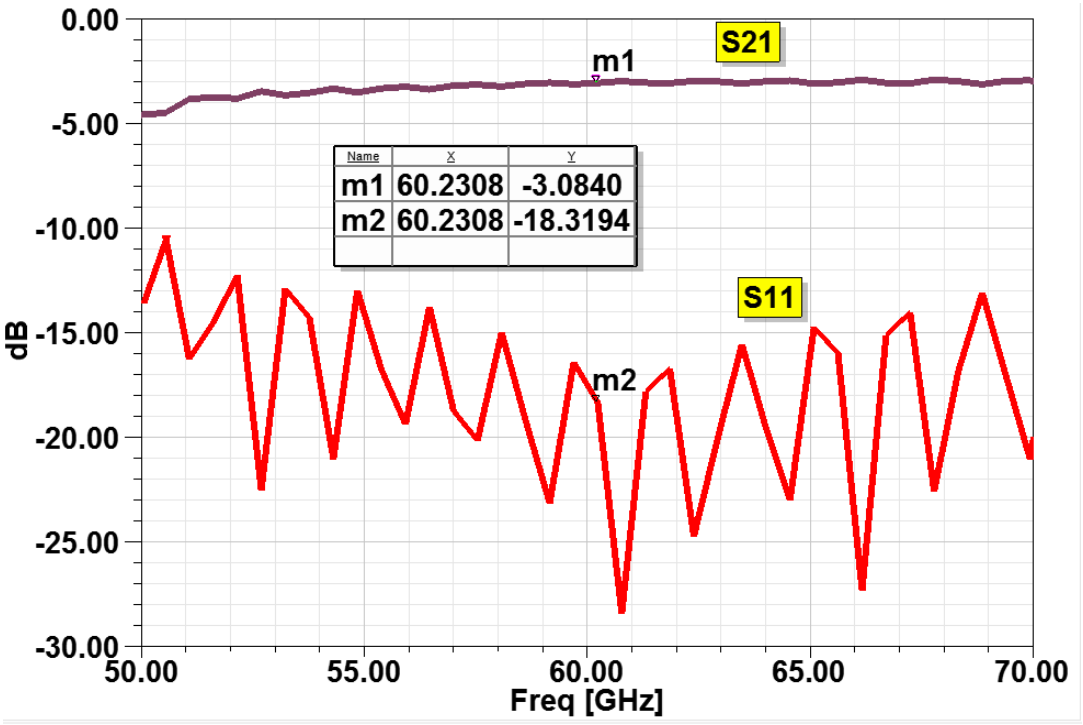
S21
m1
S11
m2
Name | X | Y
m1 | 60.2308 | -3.0840
m2 | 60.2308 | -18.3194
0.00
-5.00
-10.00
-15.00
-20.00
-25.00
-30.00
dB
50.00
55.00
60.00
65.00
70.00
Freq [GHz]

©

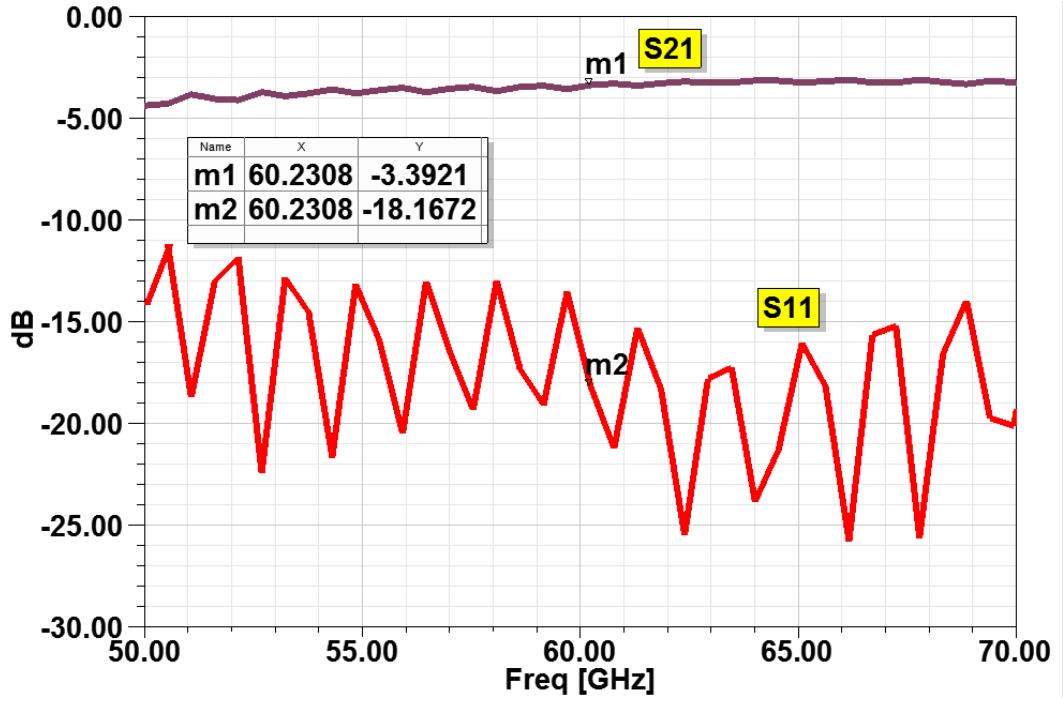
S21
m1
S11
m2
Name | X | Y
m1 | 60.2308 | -3.3921
m2 | 60.2308 | -18.1672
0.00
-5.00
-10.00
-15.00
-20.00
-25.00
-30.00
dB
50.00
55.00
60.00
65.00
70.00
Freq [GHz]

(d)

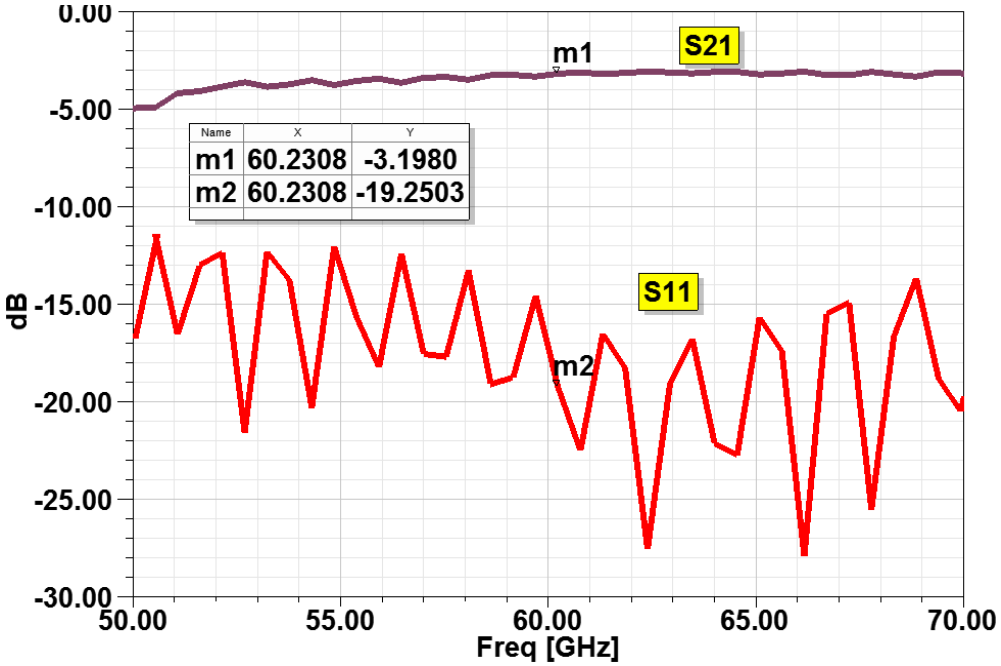

(e)

Figure 2.10: S11 and S21 of the 60GHz SIW vs frequency for 0.25mm thick alumina substrate: (a) SIW with microstrip line and λ/4 taper transition; (b) SIW with microstrip line and λ/2 taper transition; (c) SIW with microstrip line and 3λ/4 taper transition; (d) SIW with microstrip line and 5λ/4 taper transition; © SIW with microstrip line and 7λ/4 taper transition.

2.4 Fabrication Process

The sketch of the final device is shown in figure 2.11. The length of the SIW is 21mm, and 2 rays of 30 holes will be drilled on the alumina substrate to form this structure. Considering the dimensions of the microstrip lines and the taper transitions, the total length of the substrate is 29mm and the width is 4mm.

For the fabrication, first a 2 inches by 2 inches alumina sheet was cut into 5 pieces of 29mm by 4mm alumina substrate, then 2 arrays of 30 holes was drilled on the alumina substrate. After that the top surface and the ground plane were coated by sputtering with Platinum.

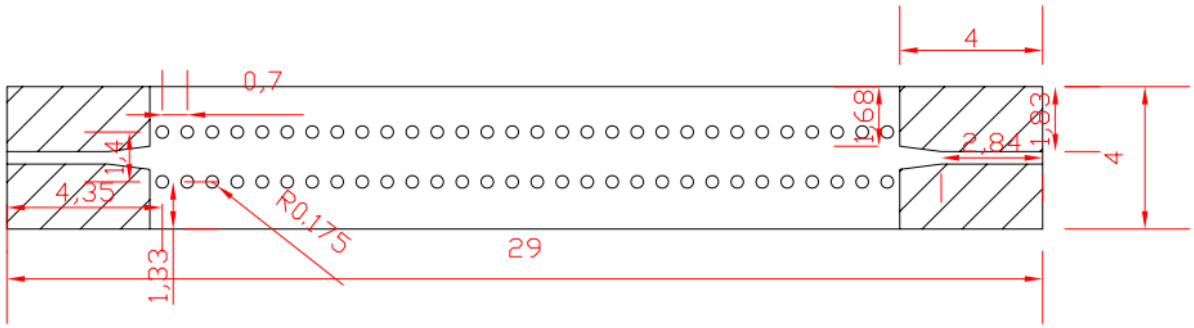

Figure 2.11: Sketch of SIW on a 0.25mm thick alumina substrate.

To make a successful 60GHz isolator, several tests need to be done before the fabrication process. Since the holes will be drilled on the alumina substrate by laser processing, the first test is to see whether the laser drilling will cause any damage, including cracks in the the substrate, a pair of holes (d=0.35mm, s=0.35mm) are drilled on a 0.25mm thick alumina substrate by Laser Processing Technology Inc. Pictures of the holes on the substrate taken by microscope are shown in figure 2.12.

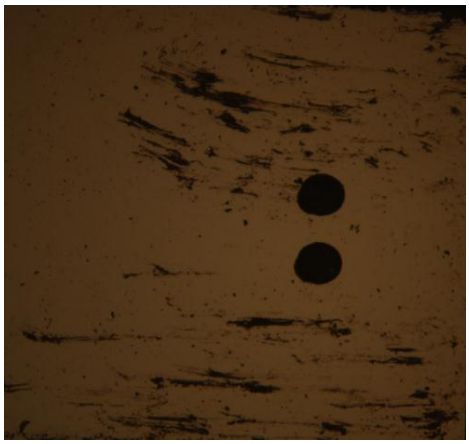

(a)

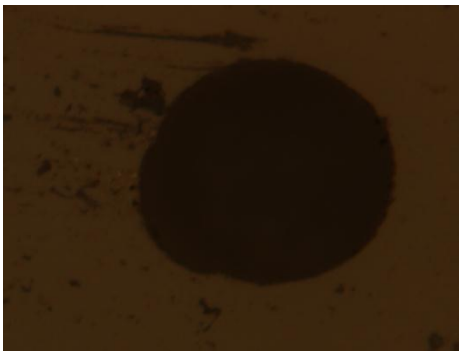

(b)

Figure 2.12: (a) Drilling holes on 0.25mm thick alumina substrate by laser; (b) a detail look of d=0.3mm hole.

Figure 2.12 shows that the holes edge is smooth and without any cracking due to the laser drilling. But one problem about laser drilling is that this process will create some scratches on substrate surface, as is shown in figure 2.12 (a).

The second test is to prove that most of the surface roughness is caused by the laser processing process. The nanofabrication will not cause any damage to the device. To prove this, a test on alumina substrate using ion milling is performed. The ion mill test

shows that the etching rate of alumina is about 5A/min, which is much slower than the etching rate of Platinum. Compares to the laser drilling results in figure 2.12, it is found that the damage caused by ion mill is much less than by laser drilling.

The third test is coating a Platinum layer on d=0.35mm holes. This test is to see whether we can make the entire hole surface be covered by Platinum by sputtering. Because the holes need to be conducting, this step can help us to see whether the sputter process will deposit Pt over the walls of the holes.

The third test was successful on a 0.25mm thick alumina substrate. The alumina substrate used in the first test was coated with Pt. The size of the substrate is 29mm by 4mm, which is as same as the 60GHz SIW. And the dimensions of the holes are also the same. A 50nm thick Platinum layer is sputtered on this substrate, all the surface especially the sidewalls inside the holes were coated successfully. DC test shows that the holes are conducting after the sputter test. The coating result is shown in figure 2.13.

Figure 2.13: Platinum sputter result on alumina substrate with d=0.35mm holes.

The final substrate is shown in figure 2.14. To avoid the skin effect losses [48], the substrate is coated with a 1um Platinum layer. The equation used for the thickness calculation is:

$$\delta_s = \sqrt{1/\pi f \mu \sigma} \tag{2.12}$$

The thickness of the Platinum layer should be larger than the skin depth δs.

Figure 2.14: The 60GHz SIW with microstrip lines and taper transitions.

2.5 60GHz Test Platform

Since the length of the 60GHz SIW is less than 3cm, it will be difficult to directly connect the device to the test equipment. So a test platform is designed. The 1.85mm connectors are soldered on the test platform instead of the device. The sketch of the test platform is shown in figure 2.15. The 60GHz device will be inserted into the holes of the test platform. 1.85mm connectors are soldered on the microstrip lines of the test platform. The top surface of the device will be connected to the conductor of the microstrip lines on the test platform, while the ground plane of the device will be connected to the ground plane of the microstrip lines of the test platform. Besides, the test platform can be used in other 60GHz tests without soldering the connectors.

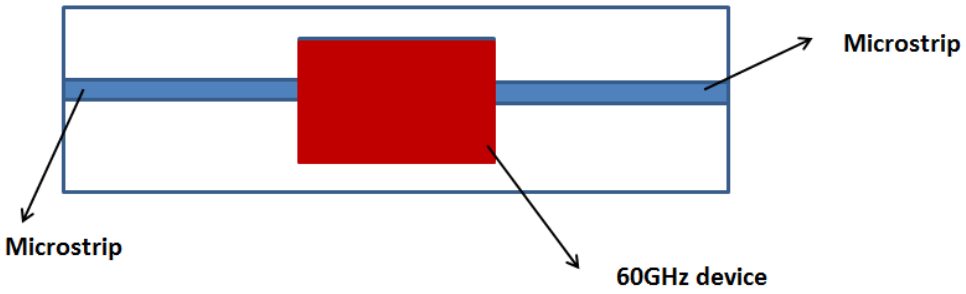

(a)

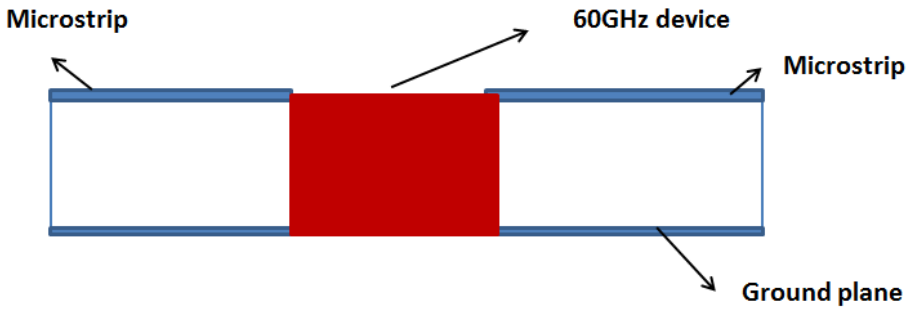

(b)

Figure 2.15: (a) The top view of the test platform; (b) the side view of the test platform.

The microstrip lines are first designed for test platform. To make a larger microstrip line on the test platform, Rogers RT5880 (εr=2.2) substrate is used for design and fabrication. According to Linecal (Agilent.Inc), the microstrip line width is 1.28mm on a 0.38mm thick Rogers RT5880 substrate, and both fT and fc will be larger than 60GHz in this case. The microstrip line dimensions are shown in figure 2.16.

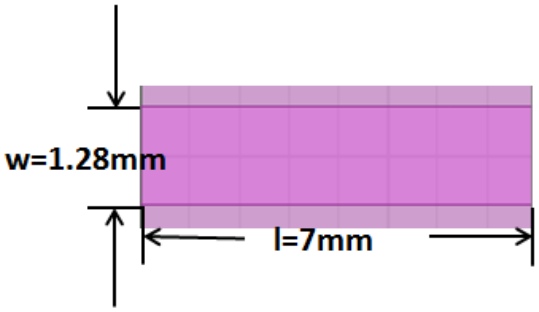

Figure 2.16: Microstrip line dimensions for Rogers 5080 substrate at 60GHz

However, the simulation result at 60GHz in HFSS is not successful. The reason is that in HFSS, the simulation result on microstrip line depends on the port size, the result

varies with the change of port size. How to set a suitable port size is the key to get a successful simulation result in HFSS. On one hand, to get a reasonable simulation result, usually the port width should be at least 3 times of the microstrip line width, and the port height should be at least 4 times of the microstrip line height. So a large microstrip line means a large port size. On the other hand, with the working frequency increases, the port size can be used in HFSS decreases and there is a port size limit in HFSS. If the port size is beyond the software limit, HFSS will return an incorrect simulation result. The port size limit makes it to be impossible to get a successful result for 60GHz on Rogers RT5880, because the microstrip line width is too large, which means the port size in this case will be too large to be used in HFSS.

To get a reasonable simulation result, a scale model is used in HFSS. It is known when that the geometry model changes, the working frequency will also change by the same ratio [72]. As a result, we can use a scale model working at 10GHz in HFSS by scaling up the 60GHz geometry model. If the scale model at 10GHz works in HFSS, the 60GHz geometry model will also work.

In this case, considering the substrate is RT5880 (εr=2.2), the width (wms) depends on the substrate thickness and characteristic impedance (Z0), only line length (lms) influences the working frequency. At 60GHz, 2π phase shift is about 3.5mm, scaling it up by a factor of 6, line length becomes 21mm and working frequency drops to 10GHz. The dimensions and the simulation results for 10GHz microstrip line are shown in figure 2.17.

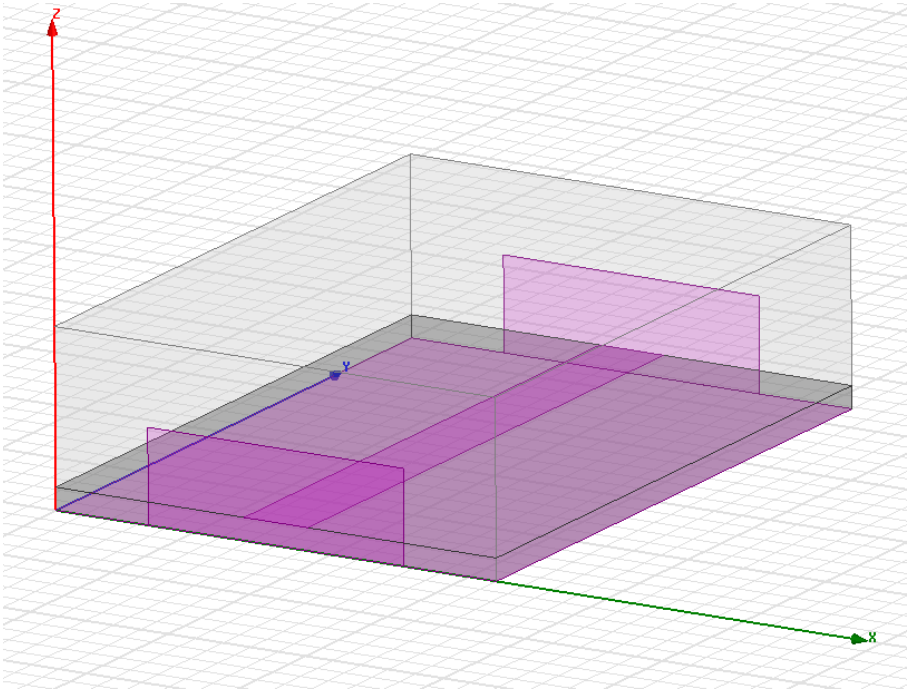

(a)

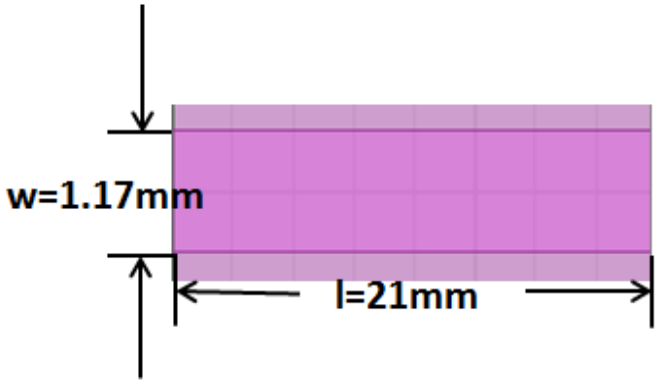

(b)

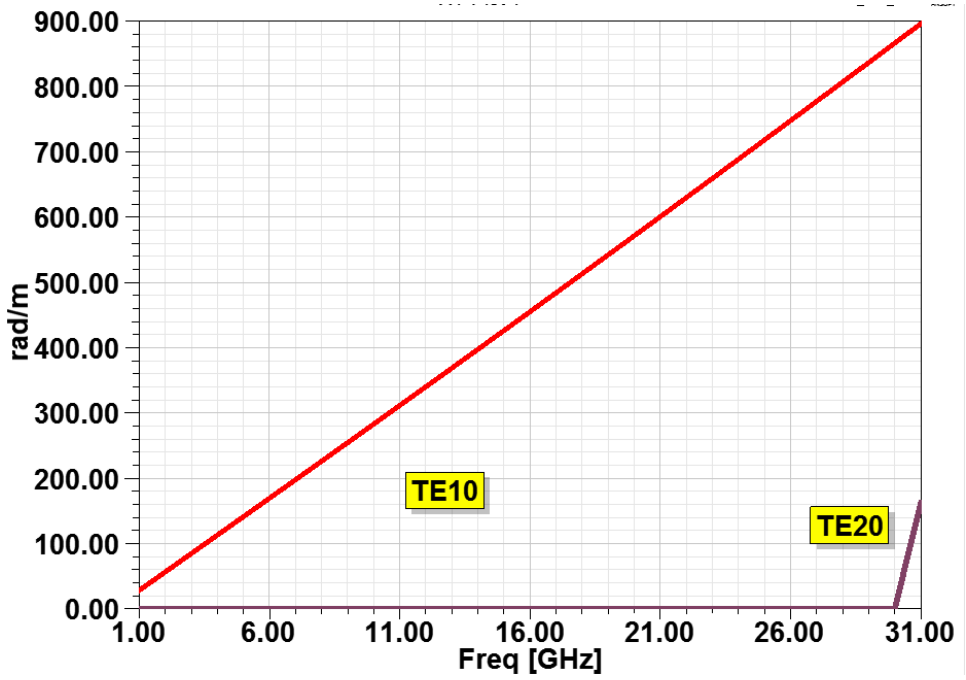
900.00
800.00
700.00
600.00
500.00
400.00
300.00
200.00
100.00
0.00
rad/m
TE10
TE20
1.00
6.00
11.00
16.00
21.00
26.00
31.00
Freq [GHz]

©

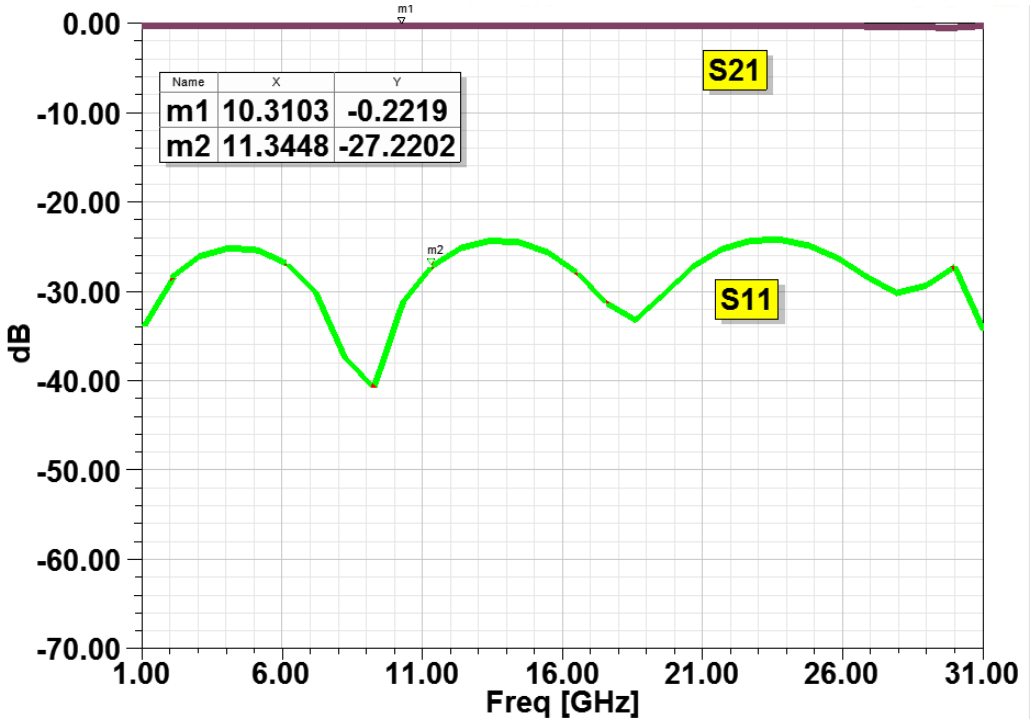
m1
0.00
-10.00
-20.00
-30.00
-40.00
-50.00
-60.00
-70.00
dB
Name
X
Y
m1
10.3103
-0.2219
m2
11.3448
-27.2202
S21
m2
S11
1.00
6.00
11.00
16.00
21.00
26.00
31.00
Freq [GHz]

(d)

Figure 2.17: (a) 10GHz microstrip line on a 0.38mm thick Rogers 5080 substrate; (b) microstrip line dimensions; (c) propagation Constant TE_{m0} vs frequency;(d) S_{11} and S_{21} vs frequency

Simulation results in figure 2.17 show that the microstrip line (w_ms=1.17mm, l_ms=21 mm) could be used at 10GHz. According to the discussion before, the 10GHz simulation results in figure 2.17 imply that the microstrip line in figure 2.16 (wms=1.28mm, lms=7mm) would work successfully at 60GHz.

Since the SIW alumina chip is 29 mm long and 4 mm wide, the size of the test platform is set to be 43mm by 8mm. A central slot will be cut in the substrate to drop the device chip in it. The ground plane of the test fixture will be extended to join the ground plane of the 60GHz device in the slot using copper tape. The microstrip lines of the test fixture will also be connected to the chip microstrip lines. The dimensions of the platform structure are shown in figure 2.18.

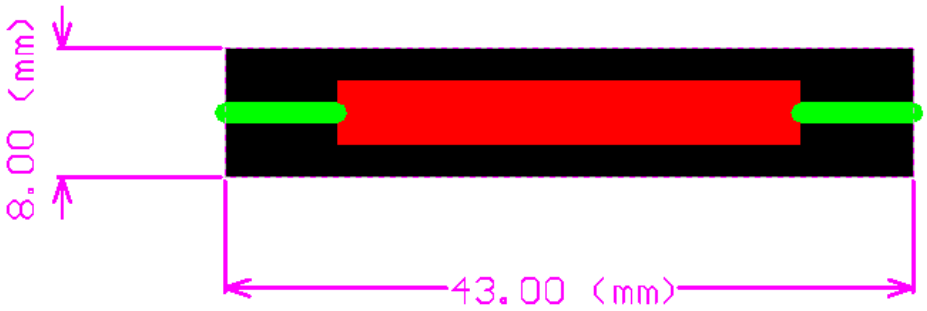

(a)

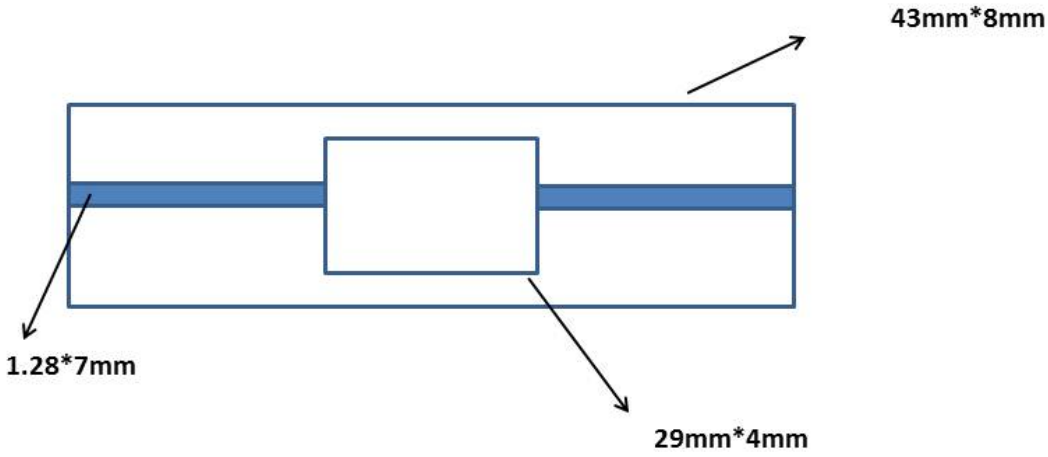

(b)

Figure 2.18: (a) Altium design for isolator test platform; (b) test platform dimensions.

The 60GHz test platform is made by a milling machine. Two 1.85mm connectors are soldered on the microstrip lines of the platform. The picture of the test platform is shown in figure 2.19.

Figure 2.19: The 60GHz test platform with 1.85mm connectors

2.6 Results and Discussion

The performance of 60GHz SIW is tested by 67GHz R&S ZVA vector network analyzer (Rohde & Schwarz Inc.).

The return loss is shown in figure 2.20. The return loss shows the power reflected in the measurement system. The equation of return loss is:

$$RL(dB) = 10log_{10}\frac{P_i}{P_r} \tag{2.13}$$

Here, Pi is the incident power and Pr is the reflected power

For the 60GHz SIW, the return loss is under -20dB.

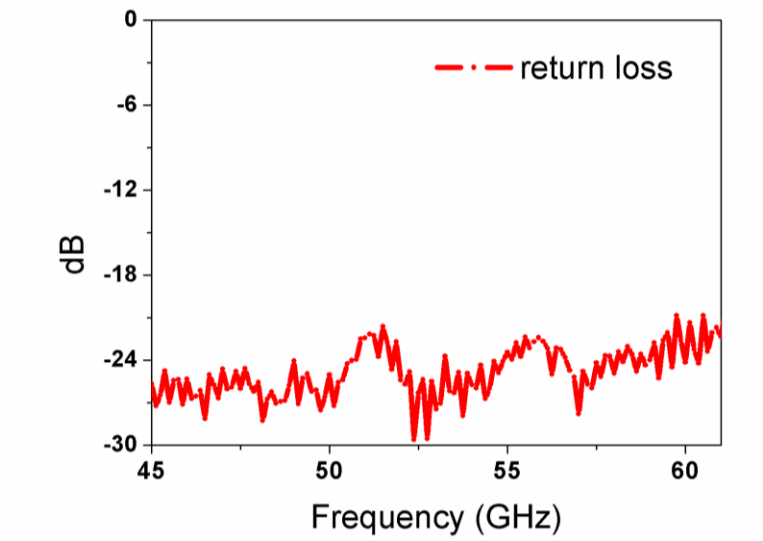

Figure 2.20: Return loss of the 60GHz SIW

The insertion loss of the 60GHz SIW with test platform is shown in figure 2.21. The insertion loss shows the power loss caused by the SIW during the transmission. The equation is:

$$IL(dB) = 10log_{10}\frac{P_t}{P_r} \tag{2.14}$$

Here, Pt is the power transmitted to the load.

For the 60GHz SIW, measurement result shows that the insertion loss is about -8dB.

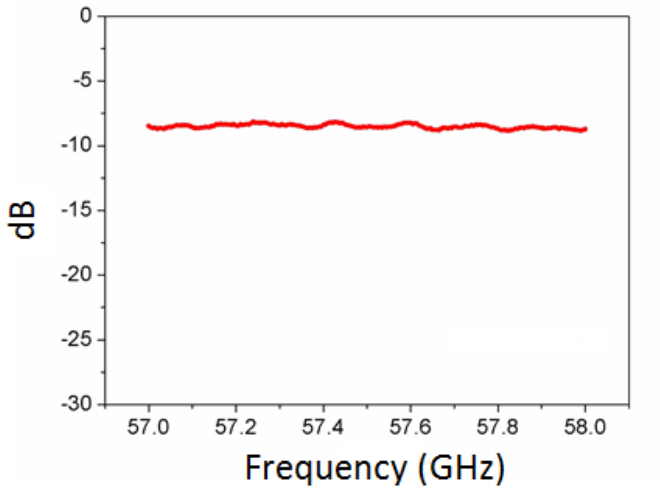

Figure 2.21: Insertion loss of test platform with 60GHz isolator

The insertion loss in figure 2.21 looks large for a 60GHz device. But a deep thinking into the results find out that the insertion loss is combined by two parts: the insertion loss of the 60GHz device and the insertion loss of the 60GHz test platform. Therefore, the test result in figure 2.21 doesn't give the insertion loss of the 60GHz device.

Since the device is connected with the 60GHz platform during the test, the insertion loss of the test platform is measured. Figure 2.22 is the test platform with 60GHz microstrip line. According the test result in figure 2.23, the insertion loss of the 60GHz test platform is about -3 dB. Figure 2.21 shows that the total insertion loss is about -8dB. Considering about the insertion loss of the test platform in figure 14 (-3 dB) and the copper tape transitions (about -1 dB), the insertion loss of the 60GHz SIW is about -4dB, which meets the simulation results of the 60GHz SIW with microstrip lines and taper transitions in figure 2.10.

Figure 2.22: Test platform with 60GHz microstrip line

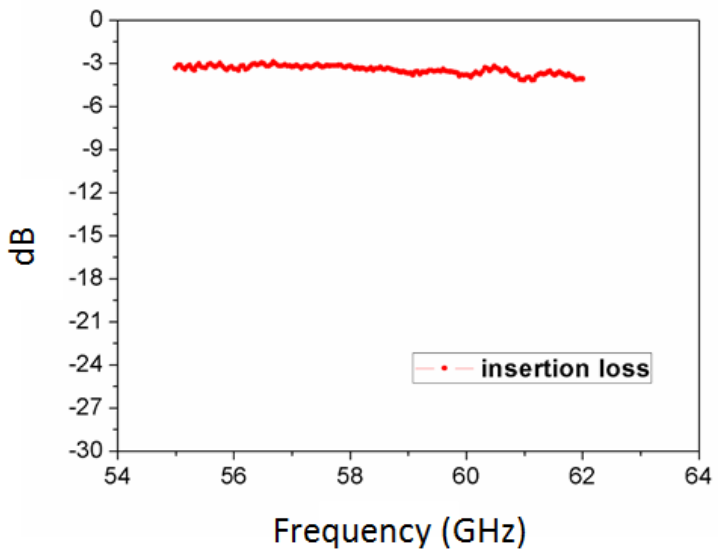

Figure 2.23: Insertion loss of test platform with 60GHz microstrip line

A summary of the measurement results is shown in table 1. Based on the measurement results, it can be found that the 60GHz SIW works functionally at 60GHz, and the test results in accordance with the simulation results. As a result, the 60GHz SIW can be used as the transmission line of 60GHz devices.

Insertion loss of 60GHz device with test platform	-8 dB
Insertion loss of 60GHz test platform	-4 dB
Insertion loss of 60GHz device	-4 dB
Return loss of 60GHz device	Under -20 dB

Table 2.1: Summary of test results on 60GHz isolators

CHAPTER 3

THE 60GHZ ISOLATOR BASED ON SIW

An ideal isolator is a two-port device where low loss transmission only occurs in one direction. The S matrix of isolator is [73]:

$$S = \begin{pmatrix} 0 & 0 \\ 1 & 0 \end{pmatrix} \tag{3.1}$$

In this chapter, a 60GHz planar isolator based on SIW is designed and its performance is measured.

3.1 The Principle of Isolators

According to the Maxwell's equations, the magnetic flux density B is a response to the magnetic field intensity H by[48]:

$$\vec{B} = \mu\vec{H} \tag{3.2}$$

where, μ is the permeability of the material. Depending on the different responses, materials can be classified as: 37 aramagnetic, ferromagnetic, ferrimagnetic and diamagnetic [74]. The isolator is a ferrimagnetic device. Ferrites are polycrystalline magnetic oxides, and there are mainly three kinds of ferrites: the spinels, the garnets and the hexagonal ferrites [75]. Among them, hexagonal ferrites are used mostly for millimeter wave applications.

For a ferrimagnetic material, the magnetic moments have different directions, but when a DC biased magnetic field is applied, the moment of the magnetic dipole will change [76]. The DC external field H0 will first bring a torque to the magnetic dipole:

$$\vec{T} = \vec{m} \times \overrightarrow{B_0} = -\mu_0\gamma\vec{s} \times \overrightarrow{H_0} \tag{3.3}$$

where, m is the moment, γ is the gyromagnetic ratio and $\vec{s}$ is the spin angular momentum.

Note that torque can be also expressed as:

$$\frac{d\vec{s}}{dt} = \frac{-1}{\gamma}\frac{d\vec{m}}{dt} = \vec{T} = \mu_0 \vec{m} \times \overrightarrow{H_0} \tag{3.4}$$

Then,

$$\frac{d\vec{m}}{dt} = -\mu_0 \gamma \vec{m} \times \overrightarrow{H_0} \tag{3.5}$$

For N unbalanced electro spins, the net magnetization is:

$$\vec{M} = N\vec{m} \tag{3.6}$$

As a result, formula becomes:

$$\frac{d\vec{M}}{dt} = -\mu_0 \gamma \vec{M} \times \vec{H} \tag{3.7}$$

where $\vec{H}$ is the internal applied field.

When the magnetic bias is applied to an un-magnetized ferrite, with the biased field increase, the magnetization M will also increase until a saturation Ms is achieved. And beyond this point, M will not change. So for ferrite, formula is:

$$\vec{B} = \mu_0(\vec{H} + \vec{M}) \tag{3.8}$$

In CGS system, it is:

$$\vec{B} = \vec{H} + 4\pi\vec{M} \tag{3.9}$$

When $\vec{H}$ is an AC field, the total magnetic field is:

$$\overrightarrow{H_{total}} = \overrightarrow{H_{DC}} + \overrightarrow{H_{RF}} \tag{3.10}$$

Assume that HDC is in z direction, the magnetization becomes:

$$\overrightarrow{M_{total}} = M_s\hat{z} + \vec{M} \tag{3.11}$$

In tensor form one can get:

$$\vec{M} = [\chi]\vec{H} = \begin{bmatrix} \chi_{xx} & \chi_{xy} & 0 \\ \chi_{yx} & \chi_{yy} & 0 \\ 0 & 0 & 0 \end{bmatrix}\vec{H} \tag{3.12}$$

[χ] is the tensor susceptibility. As a result, for ferrite with an AC magnetic field and a bias in z direction, permeability is also a tensor form:

$$[\mu] = \begin{bmatrix} \mu & j\kappa & 0 \\ -j\kappa & \mu & 0 \\ 0 & 0 & \mu_0 \end{bmatrix} \tag{3.13}$$

$$\mu = \mu_0(1 + \frac{\omega_0\omega_m}{\omega_0^2-\omega^2}) \tag{3.14}$$

$$\kappa = \mu_0\frac{\omega_0\omega_m}{\omega_0^2-\omega^2} \tag{3.15}$$

From the formulas, it is found that the tensor permeability depends on the frequency, Ms and H_0.

When a plane wave is propagating in the ferrite, if the propagation is in the direction of the bias, it is called the Faraday rotation [77]. When the rotation is transverse to the bias, two solutions exist. The first solution is not affected by the H_0 and is called the ordinary wave. The second solution is affected by the ferrite and propagation constant becomes:

$$\beta_e = \omega\sqrt{\mu_e\epsilon} \tag{3.16}$$

And the effective permeability is given by:

$$\mu_e = \frac{\mu^2 - \kappa^2}{\mu} \tag{3.17}$$

For a ferrite loaded rectangular waveguide shown in figure 3.1, considering that the TE mode wave is propagating in the medium.

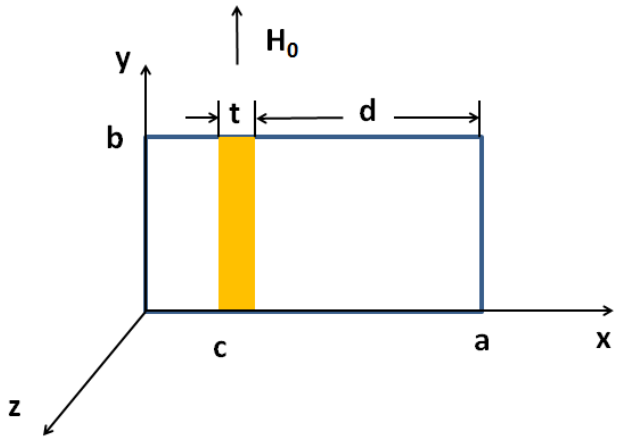

Figure 3.1: Ferrite-loaded rectangular waveguide

In this case, e_z =0 and ∂/∂y=0, applying Maxwell's equations, the following general solutions are got:

$$e_y = \begin{cases} Asink_a x & for\ 0 < x < c \\ Bsink_f(x-c) + Csinkf(c+t-x) & for\ c < x < c+t \\ Dsink_a(a-x) & for\ c+t < x < a \end{cases} \tag{3.18}$$

$$h_z = \begin{cases} (jk_a A/\omega\mu_0)cosk_a x & for\ 0 < x < c \\ (j/\omega\mu\mu_e)\{\kappa\beta[Bsink_f(x-c) + Csink_f(c+t-x)]\} & for\ c < x < c+t \\ (-jk_a D/\omega\mu_0)cosk_a(a-x) & for\ c+t < x < a \end{cases} \tag{3.19}$$

Where, k_a is the cutoff wavenumber in the air region and k_f is the cutoff wavenumber of the ferrite:

$$k_f^2 = \omega^2 \mu_e \epsilon - \beta^2 \tag{3.20}$$

$$k_a^2 = k_0^2 - \beta^2 \tag{3.21}$$

By applying the boundary conditions, ABCD can be substituted and eliminated, and the transcendental equation for propagation constant β is:

$$\left(\frac{k_f}{u_e}\right)^2 + \left(\frac{k\beta}{uu_e}\right)^2 - k_a cotk_a c\left(\frac{k_f}{u_0 u_e} cotk_f t + \frac{k\beta}{u_0 uu_e}\right) - \left(\frac{k_a}{u_0}\right)^2 \times cotk_a ccotk_a d\left(\frac{k_f}{u_0 u_e} cotk_f t - \frac{k\beta}{u_0 uu_e}\right) = 0 \tag{3.22}$$

An approximate result is:

$$\beta_+ - \beta_- \approx 2k_c \frac{\kappa}{\mu}\frac{\Delta S}{S} sin2k_c c \tag{3.23}$$

Where, β+-β- is the difference between the phase shift, ΔS/S is the filling factor and kc=π/a is the cutoff frequency of the empty waveguide.

And the forward attenuation constant α+ and the reverse attenuation constants α- can be expressed as:

$$\alpha_{\pm} \simeq \frac{\Delta S}{S\beta_0}(\beta_0^2 \chi''_{xx} \sin^2 k_c x + k_c^2 \chi''_{zz} \cos^2 k_c x \mp \chi''_{yy} k_c \beta_0 \sin 2k_c x) . \tag{3.24}$$

Formula (3.24) implies that the attenuation constants are determined by the ferrite load space ratio ΔS/S, the propagation constant β_0, the cutoff frequency k_c and the susceptibilities complex χ. If the ferrite slab is inserted at the optimum position inside the waveguide, the forward attenuation constant α+ will be small while the reverse constant α- will be huge, and the isolation will be achieved.

When the usual TE_{10} mode propagates in the ferrite loaded rectangular waveguide, it will have a circular polarized component with the H_x and H_z fields. An interaction with the ferrite slab now has a circular polarized wave in the same rotation direction, while in the opposite rotation direction the interaction will be much weaker. If the operation frequency is near the gyromagnetic resonance frequency, the attenuation constant will be large. However, the attenuation constant of the plane wave in the opposite direction is small. Such a device is called the resonance isolator [78].

3.2 Self- biased Thin Film Ferrite

Sometimes three-port circulator is used as an isolator, this property can be found in its S matrix [73]:

$$S = \begin{pmatrix} 0 & 0 & 1 \\ 1 & 0 & 0 \\ 0 & 1 & 0 \end{pmatrix} \tag{3.25}$$

However at 60GHz, the size of the ferrite disk becomes so small that the microstrip lines could not fit in [79]. As a result, ferrite slab loaded waveguide isolator is used.

Although some isolators have been developed using SIW technologies, most of them have low FMR. The reason is that most of the isolators use YIG ferrites. The common way to increase the working frequency of the isolator is using a large magnetic bias, in most of the cases electromagnets are employed because of the low FMR of ferrite material, which is not suitable for this project because it is not suitable for planar device and the Barium ferrite is used for 60GHz planar devices.

3.2.1 C-axis Barium (BaM) Thin Films

In order to achieve strong coupling at millimeter wave frequencies, the ferrite needs to have a large saturation magnetization value, high permeability, and narrow FMR linewidth. C-axis M-type BaM ($BaFe_{12}O_{19}$) is particularly attractive because it can be magnetically self-biasing, which allow for the design of ferrite devices working at 60GHz without the need for heavy and expensive magnets [80]. A sketch of BaM crystalline structure is shown in figure 3.2 [81].

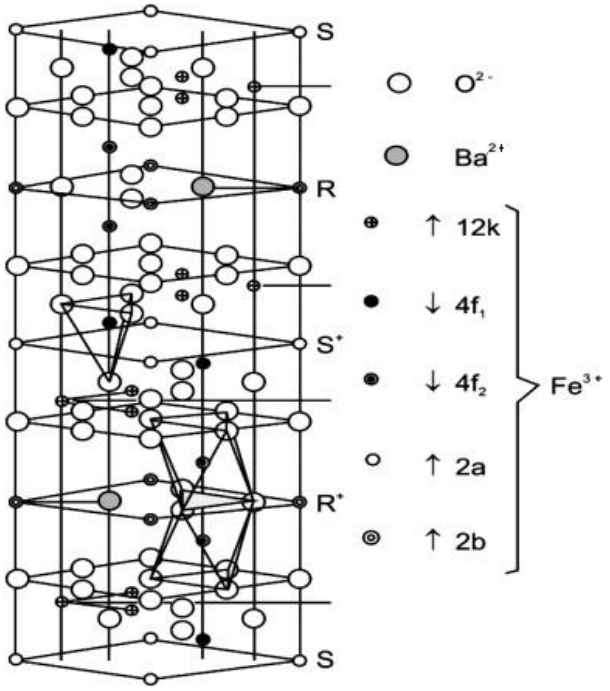

Figure 3.2: The BaM crystalline structure

The BaM thin film can be coated on the polycrystalline alumina substrates substrate by a chemical solution deposition (CSD) process. In this technique, solutions of the compounds are mixed at the desired ratio to form a coating solution. This coating solution is deposited on a substrate by dip-coating to produce a wet film, which is then heated to first remove any solvent and organic component that did not evaporate during

the deposition step and then to decompose the metal-organic or metal-salt precursors and subsequently crystallize the materials. It is found that the starting ratio of Ba2+:Fe3+ ions in the precursor solution has a significant impact on the crystallization behavior of the BaM thin films [82]. Using this technique a high quality BaM thin film can be coated on the alumina substrate (Superstrate 996, CoorsTek.Inc). The reason of using the polycrystalline alumina substrates is that it can provide minimum structural and thermal expansion mismatch between the thin film materials and substrates [83].

3.2.2 Magnetic Properties of BaM

The relationship between the magnetic field H and the magnetization M is first measured. M-H loops of BaM thin films are measured using a vibrating sample magnetometer (VSM) setup (Princeton Measurements MicroMag VSM 3900). The VSM test results are shown in figure 3.3. BaM thin film with different Ba2+:Fe3+ ratios are measured. From figure 3.3, it can be found that the highest anisotrophy filed is in figure 3.3 (a), so Ba2+:Fe3+ =1:12 is used. Here, the magnetic anisotropy is field value which aligns all the magnetization perpendicular to the easy axis. From figure 3.3 (a), it can also be found that the BaM thin film has a high anisotropy field compared to the bulk single crystal of BaM [84] since the maximum value of magnetization of BaM is 380 emu/cm^3.

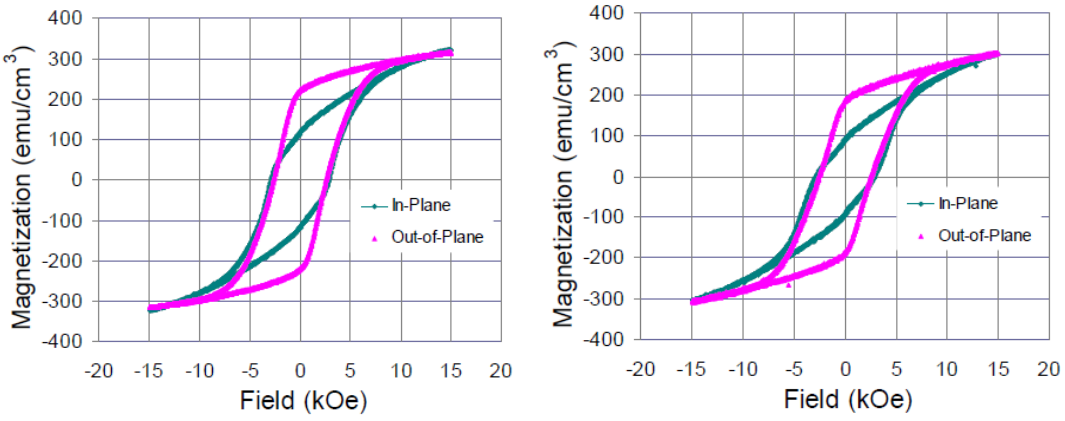

(a) (b)

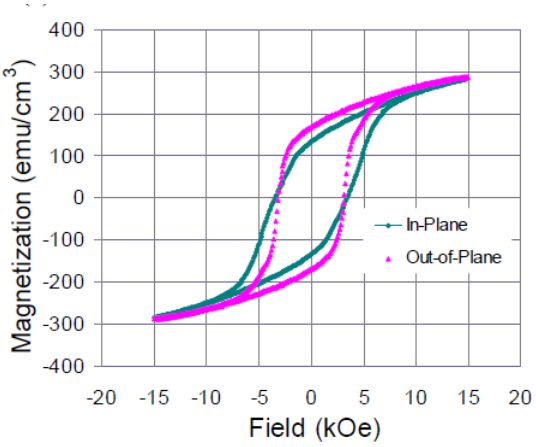

(c)

Figure 3.3: M-H loop of BaM thin film (a) with Ba2+:Fe3+ = 1:12; (b) with Ba2+:Fe3+= 1:10; (c) with Ba2+:Fe3+ = 1:8

The second test is the FMR linewidth measurement at different frequencies.

The FMR linewidth (ΔH) is fundamentally described as the imaginary part the susceptibility tensor [χ]. And the precision damping can be described as the damping

coefficient (α) in Landau-Lifshitz-Gilbert equation [85], or in half power FMR linewidth (ΔH) by the following equation:

$$\alpha = \frac{\mu\gamma\Delta H}{4\pi f} \tag{3.26}$$

The FMR test gives the RF power absorbed by the ferrites as a function of applied DC magnetic bias at a given frequency f [86].

The FMR profiles of BaM thin film at 65GHz are shown in figure 3.4. Results show that the FMR linewidths are pretty narrow, indicating relatively good quality of the thin films.

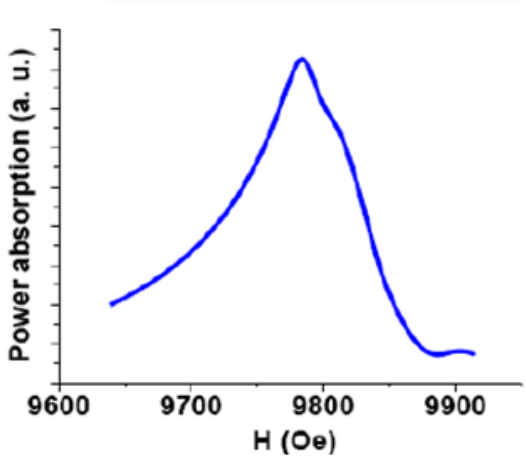

Figure 3.4: FMR linewidth of BaM thin film at 65 GHz.

Based on the improved magnetic properties, the resonance fieled H needed at working frequency f can be calculated using kittle equation [87]:

$$f = \gamma * (H + H_a - M_s) \tag{3.27}$$

For BaM thin film presented in this thesis, the saturation magnetization Ms is 4000Oe, the anisotropy field Ha is 17.2kOe, and the gyromagnetic ratio γ is 2.8 MHz/Oe. As a result, the magnetic bias needed at 60GHz is 8228Oe. Considering that the calculation result is smaller than 1 tesla, it is possible to use a small permanent magnetic to replace the bulky and expensive electromagnet for making a 60GHz ferrite isolator.

3.3 Comparison of Different Ferrite Isolators

Ferrite loaded isolators can be divided into resonance isolator and field displacement isolator. Based on the geometry of the ferrite slab, the resonance isolator can be classified as E-plane resonance isolator and H-plane resonance isolator. The performance of these three isolators will be compared to choose the best one at 60GHz.

3.3.1 E-plane Resonance Isolator

The first choice is to use an E-plane resonance isolator. The E-plane resonance isolator has a full height ferrite slab inside the waveguide. Because of the demagnetization factors, the operating frequency of the E-place isolator is smaller than the H-plane isolator. The following formula is used to obtain the operating frequency for E-plane isolator [21]:

$$f = \sqrt{f_0(f_0 + f_m)} \tag{3.28}$$

Here, f is the working frequency, which is 60GHz in this case, f_0 is the operating frequency, f_m depends on the saturation magnetization. Assume the saturation magnetization is 4000G, f_m is about 22.4GHz, f_0 is about 53.4GHz. As a result, the magnetic bias for BaM thin film ferrite is 7322Oe.

To simplify the simulation, an air filled waveguide is used. The dimensions of 60GHz waveguide are: width=4mm, thickness=2mm. According to the calculation, the ferrite width is about 0.004mm, and the optimum position of the ferrite slab is set to be 0.854mm away from the waveguide edge. The 60GHz E-plane isolator is shown in figure 3.5.

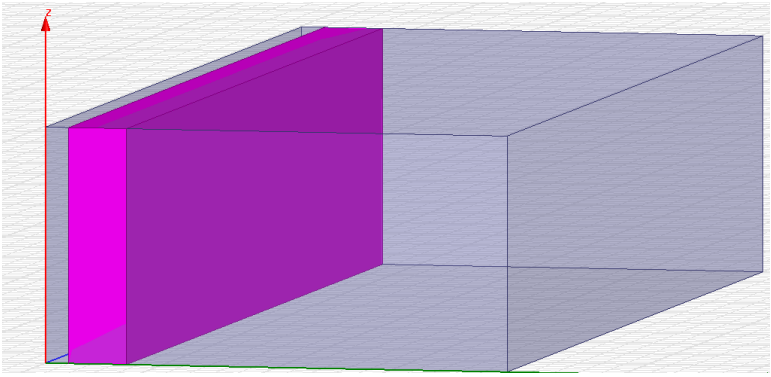

Figure 3.5: 60GHz E-plane waveguide

A drawback of using HFSS simulation is that the ferrite simulation takes too much memory., If the ferrite slab is too large, the simulation will run a long time and therefore, the ferrite slab length is set to be 1mm in the simulation, while the typical length is 2cm. The simulation result is figure 3.6 implies that the E-plane isolator works functionally at 60GHz.

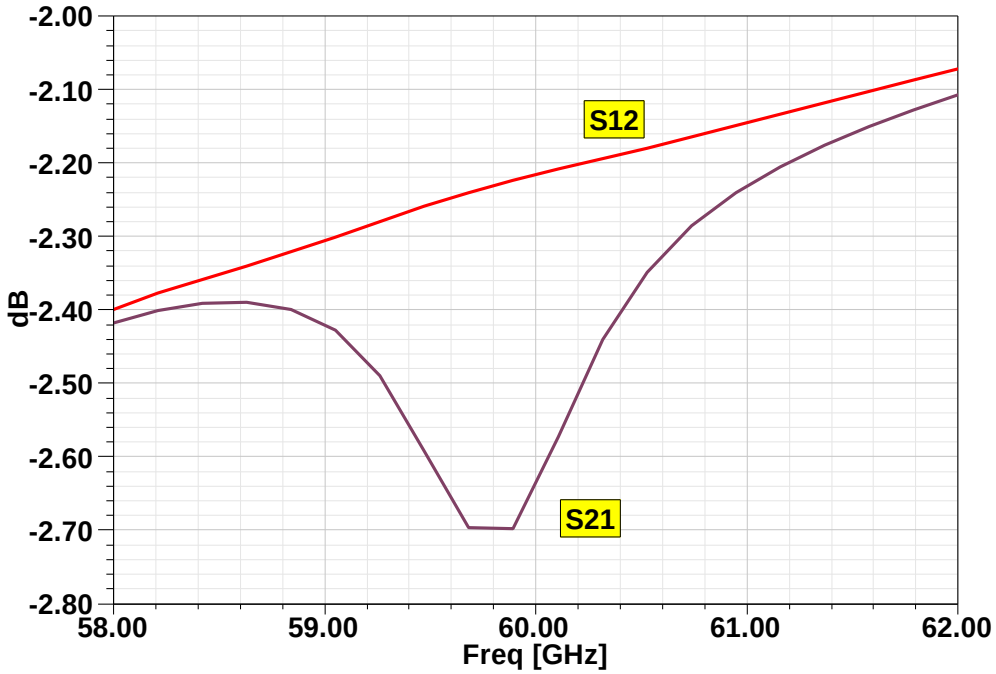

Figure 3.6: The performance of 60GHz E-plane isolator

3.3.2 H-plane Resonance Isolator

The second type is the H-plane resonance isolator. Unlike the E-plane resonance isolator, this one has a thin film ferrite slab inside the waveguide. The ferrite slab is inserted at a certain point so that the attenuation constant different directions are different. A sketch of H-plane isolator is shown in figure 3.7. The dimensions of 60GHz waveguide are: width=4mm, thickness=2mm. According to the calculation, the ferrite width is about 0.4mm, and the thickness is 0.2mm. Calculation results shows that the optimum position of the ferrite slab is set to be 1.05mm away from the waveguide edge. And at 60GHz, the DC bias is 8228 Oe.

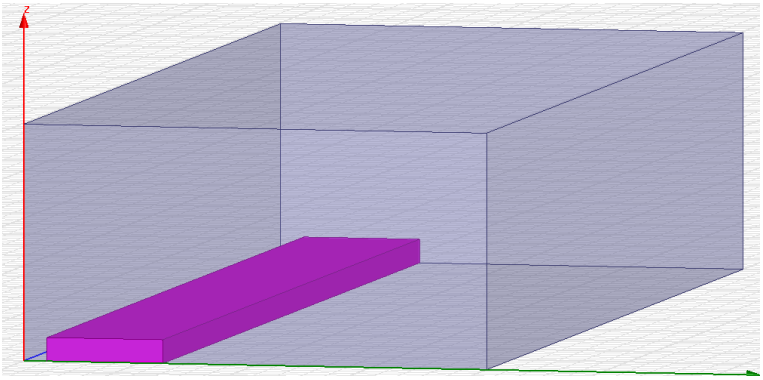

Figure 3.7: 60GHz H-plane isolator

1mm long ferrite slab is also used in field displacement isolator. The simulation result is figure 3.8 implies that the H-plane isolator works functionally at 60GHz.

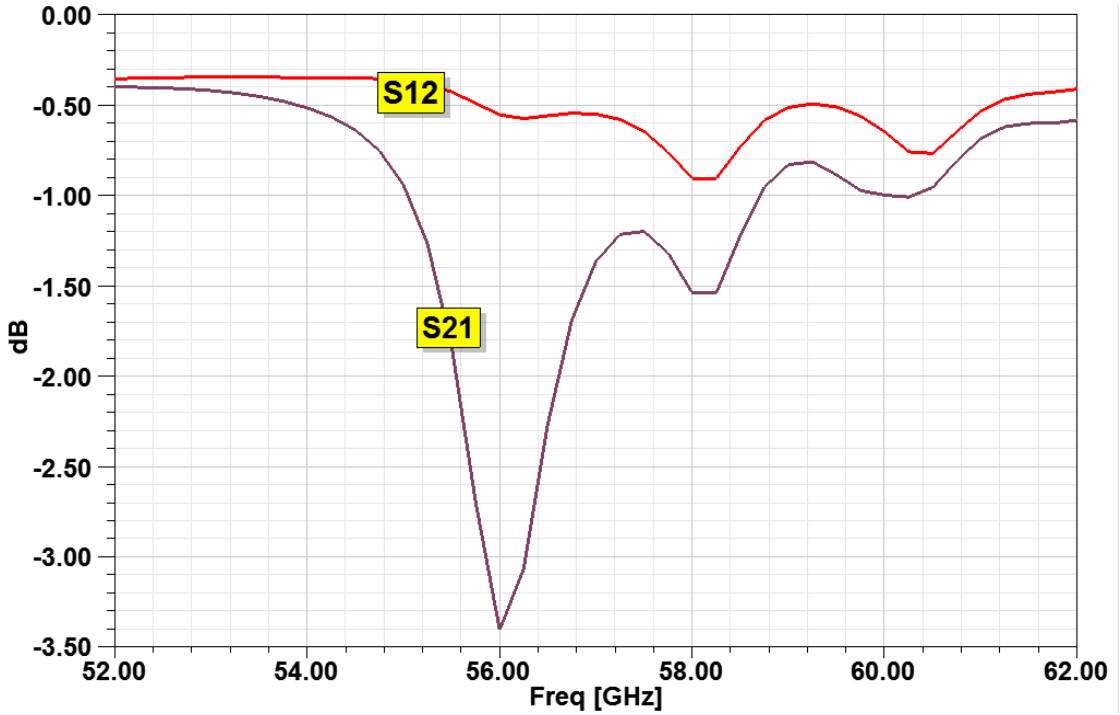

Figure 3.8: The performance of the 60GHz H-plane isolator.

3.3.3 Field Displacement Isolator

The third type is field displacement isolator. Unlike the resonance isolator, this one has a ferrite slab-loaded waveguide and a resistive sheet. The ferrite slab is inserted at a certain point so that the electric field of the forward wave is small while the electric field of the reverse wave is very large. If the resistive sheet is put next to the ferrite slab, the forward wave will be not affected; however, the reverse wave will be greatly attenuated.

Two factors need to be considered during the design stage.. The first factor is the internal bias field H_0. The internal bias field needs to be large enough to give the effective permeability $\mu_e<0$ at a certain frequency. To calculate μ_e, the following equations are used:

$$\mu = \mu_0 \left(1 + \frac{f_0 f_m}{f_0^2 - f^2}\right) \tag{3.29}$$

$$k = \mu_0 \frac{f f_m}{f_0^2 - f^2} \tag{3.30}$$

Here, the working frequency f is 60GHz, f_m is determined by the saturation magnetization, and the operation frequency f_0 can be calculated by the internal bias field H_0. The simulation result suggests that when H_0 is 11500 Oe, μ_e is imaginary at 60GHz.

Air filled isolator is also used in this case. The dimensions of 60GHz waveguide are as same as the E-plane isolator. However the ferrite slab is quite different from the resonance isolator, the ferrite width is 0.4mm, and the optimum position of the ferrite slab is about 0.1mm away from the waveguide edge. The sketch of 60GHz field displacement isolator is shown in figure.

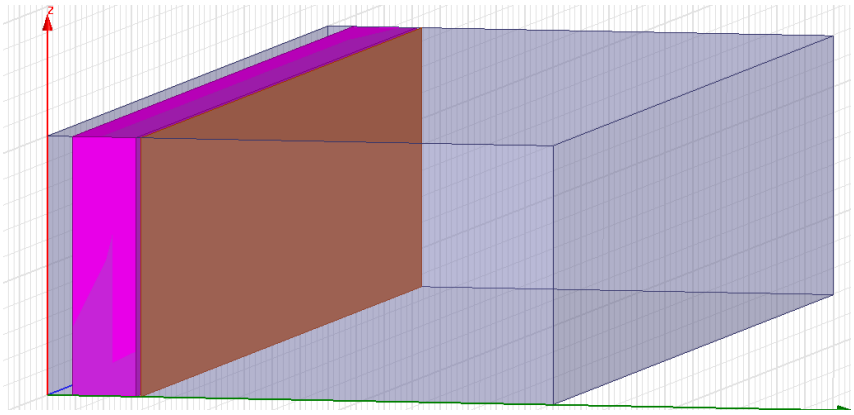

Figure 3.9: 60GHz field displacement isolator

3.9, and a 1mm long ferrite slab is also used in field displacement isolator. The simulation result is shown in figure 3.10 implies that the field displacement isolator works functionally at 60GHz.

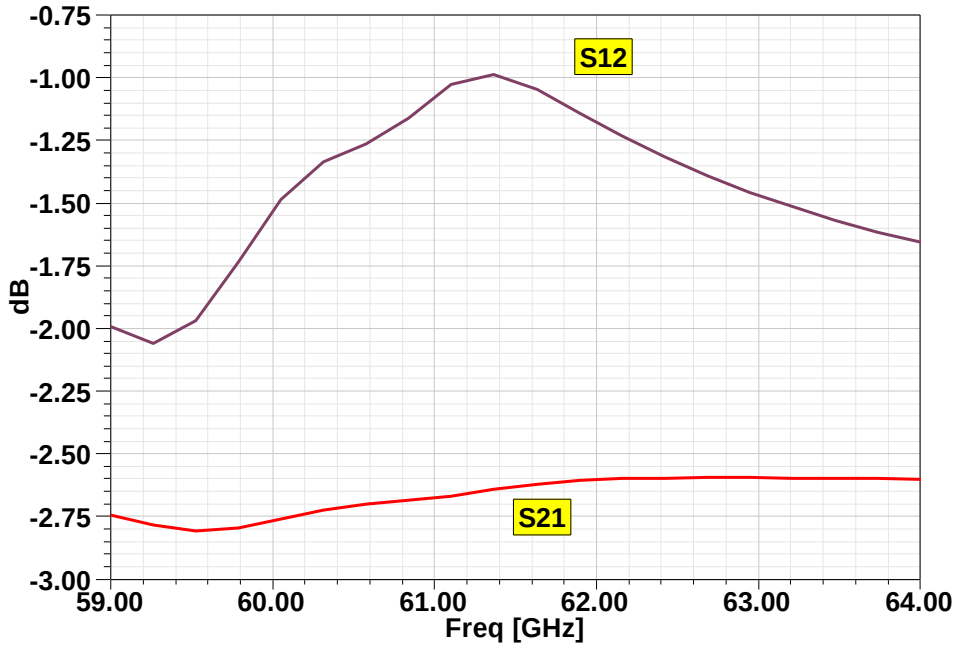

Figure 3.10: The performance of 60GHz field displacement isolator

Comparing the performance of the three different isolators, it can be found that:

1. The DC magnetic bias of the E-plane resonance isolator is the smallest because of the demagnetization factor, however the full height ferrite slab is difficult to realize in SIW.

2. The performance of the field displacement isolator is good, but to achieve an imaginary , μ_e a large DC magnetic bias is needed; besides the resistive sheet need to be placed at a precise location during the fabrication, which is difficult.

3. Compared to the other isolators, H-plane resonance isolator has the best performance and the thin film ferrite slab is easy to realize in planar structure.

Based on these conclusions, H-plane resonance isolator is used in the next step for its high performance and easy integration.

3.4 The Calculation of 60GHz H-plane Resonance Isolator

Based on the parameters of 60GHz SIW, the forward attenuation constant ($\alpha+$) and reverse attenuation constant ($\alpha-$) of the ferrite isolator at 60GHz can be calculated. However the position of the ferrite film on SIW will greatly influence the attenuation constant, as a result the optimum position of ferrite film need to be found. Assume that the width of ferrite film is 0.35mm (w/4) and the average thickness is 500nm (varies from 150nm to 1um), a model of ferrite isolator can be built as shown in figure 3.11, parameter x is the midpoint of ferrite film.

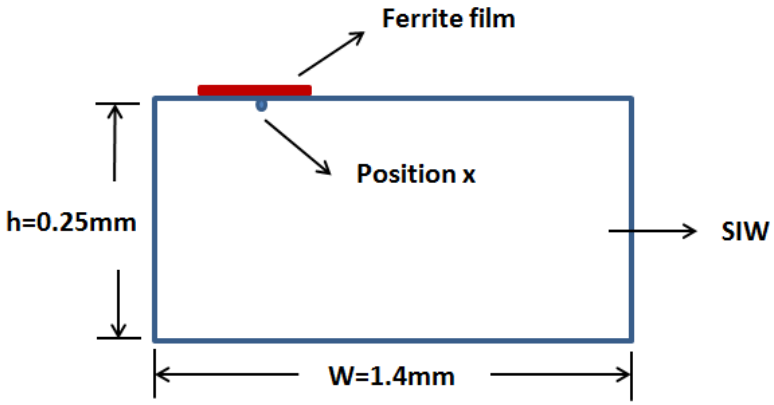

Figure 3.11: The sketch of 60GHz ferrite Isolator

Figure 3.11 shows that x varies from 0.15mm to 0.6mm. The result of attenuation constants vs x is calculated and plotted in Matlab, as shown in figure 3.12.

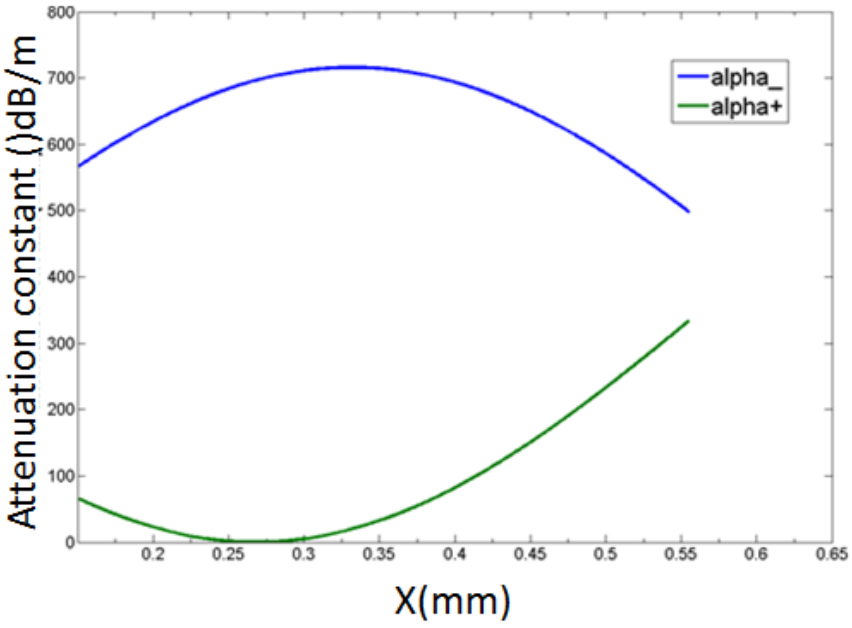

Figure 3.12: Attenuation Constants vs x

From figure 3.12, it can be found that the minimum forward attenuation constant (α+) appears at x=0.27mm. To fabricate a ferrite isolator with 10dB isolation, the length of the slab should be 21mm, and the total length of the substrate including the microstrip lines and the taper transitions is 29mm.

3.5 Fabrication

To make a 60GHz isolator based on SIW, a 0.25mm thick alumina substrate is chosen. And to reduce the loss at high frequency, Platinum is used as the metal layer. Two kinds of H-plane resonance isolators are designed to compare the performance, and they are shown in figure 3.13. The structure in figure 3.13 (a) has only one ferrite film on the top surface, while in figure 3.13 (b) the ferrite films are deposited on both the top and the bottom surface of the SIW. Because the isolation depends on the ferrite load space ratio, the two structures are expected to have different performance.

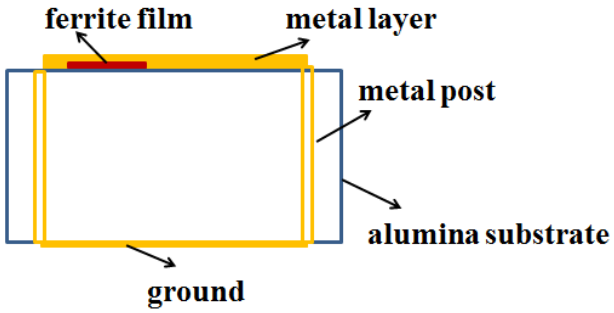

(a)

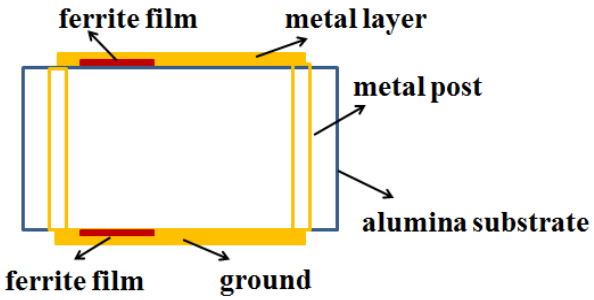

(b)

Figure 3.13: (a) H-plane resonance isolator on SIW with single sided ferrite film; (b)H-plane resonance isolator on SIW with double sided ferrite film.

The Nanofabrication Center is used to fabricate the 60GHz isolator.

The first isolator type with the ferrite slab on the top surface is first processed and the process chart is shown in figure 3.14. First, the holes are metalized by sputtering Platinum inside the holes array. To avoid the skin depth effect [48], the thickness of the Platinum layer is chosen to be at least 1um. Next a 300nm thick BaM thin film is deposited on both sides of the alumina substrate. The BaM layer is then etched to pattern the BaM ferrite thin film on SIW. For the single sided ferrite isolator, the BaM ferrite film on the bottom side is all removed while the top side is patterned with a 300nm thick ferrite strip. For double sided ferrite isolator, both sides are patterned with ferrite strips.

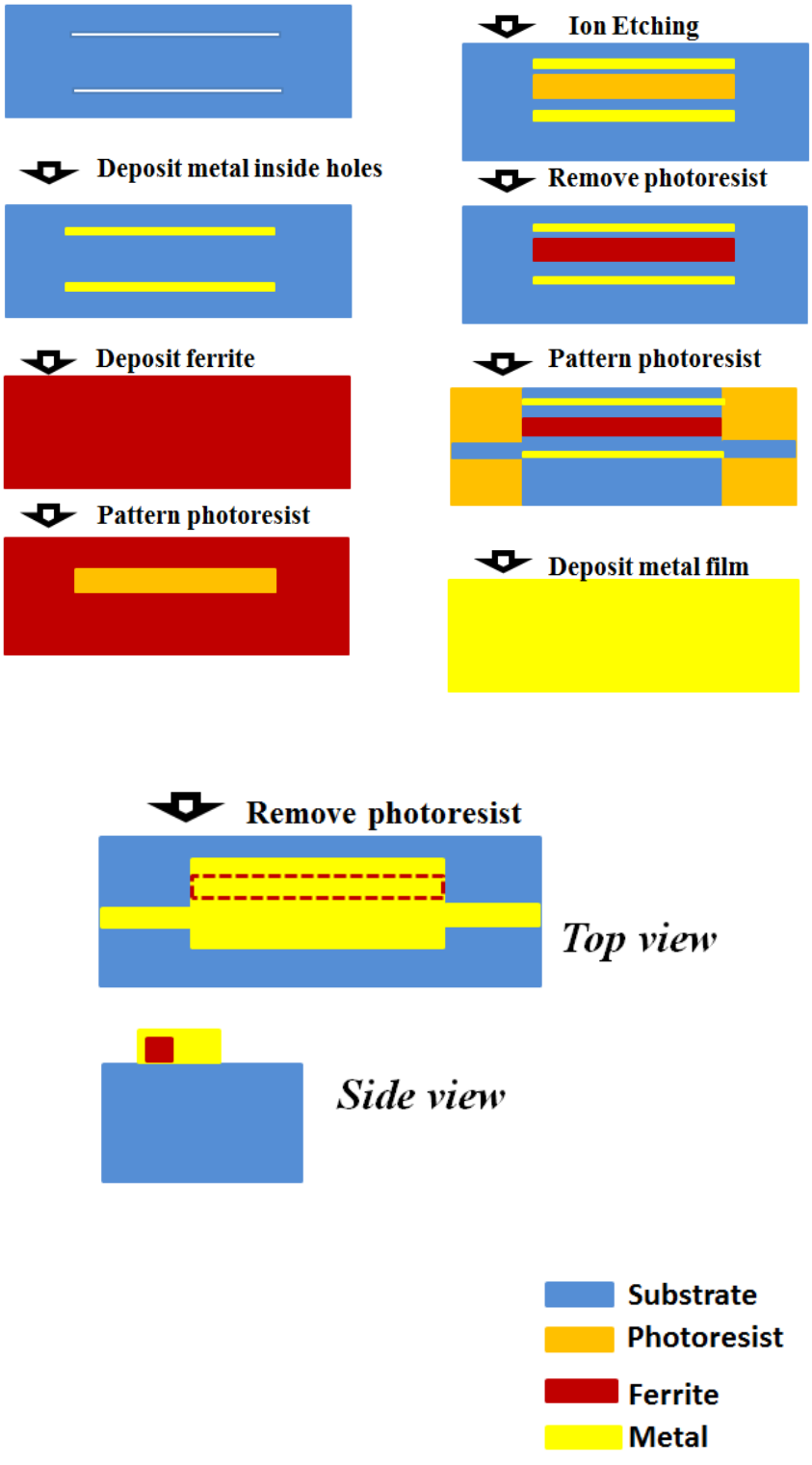

Figure 3.14: The fabrication process of 60GHz isolator based on SIW

Compared to the fabrication of 60GHz SIW, the isolator need one extra step in the fabrication, which is BaM etching. So before this fabrication step, an etching test is done on BaM thin film.

First, the reactive ion etcher (RIE) was used for this test because the literature states that the etching rate of BaM can be as high as 75nm/min [88]. However, the etching of the ferrite film in the ion etcher was not successful. The reason is that ion etching of ferrites requires a very low pressure (about 10^{-6} torr), however, the equipment in the Nanofabrication Center could not satisfy this condition.

The next test used ion mill to etch the BaM thin film. Compared to the RIE, this method normally has a much lower etching speed but it can etch almost everything. An alumina substrate with 500nm thick ferrite coating is used, a half of the sample surface is covered by photoresist (S1813). The Intlvac Nanoquest Ion Mill Etching System (Intlvac.Inc) is used for etching. The parameters are: beam V = 200 V; beam I = 70 mA; accelerate V = 24 V; etching time=30 minutes. After the etching, the photoresist is removed by acetone and the surface profile is measured. The result is shown in figure 3.15. The lower area on the left side is the ferrite film after 30 minutes ion milling, the higher area on the right side is the protected ferrite layer. The thickness difference between the etched area and the covered area is about 2200 Å. As a result the ferrite ion mill etching rate is about 70 Å/min. The noise is caused by the laser drilling roughness, the peaks on the left end are the tapes used to identify the etching area. Since the etching

rate for photoresist is about 20 Å/min under the same condition, and photoresist is much thicker than ferrite film, the ion mill method can be used for ferrite etching.

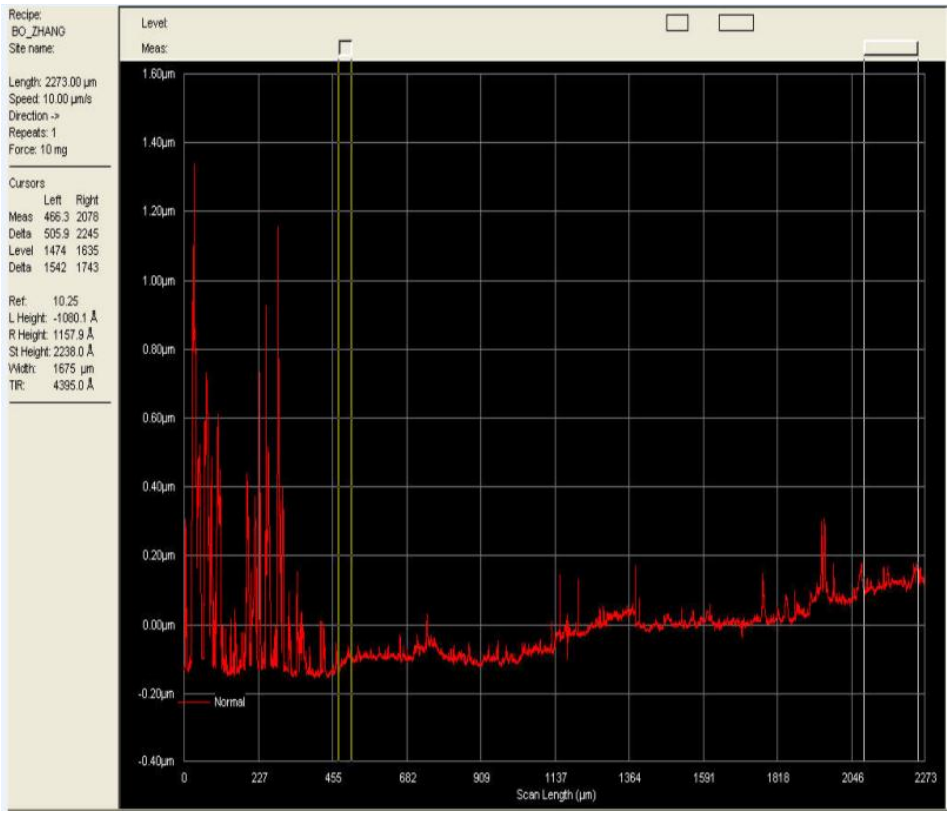

Figure 3.15: Surface profile of the alumina substrate with ferrite coating after ion mill etching

After the holes are laser filled on the 0.25 mm thick alumina substrate, a 1 um thick Platinum layer is coated inside the holes to make sure the holes are conducting. Then the BaM film is deposited on the top and bottom surfaces. A ferrite strip is retained on top surface with the ion milling, and the ferrite on bottom surface is all removed for single-side ferrite isolator. The result is shown in figure 3.16. For double-sided ferrite isolator,

the ferrite film on the back side is also patterned and the strip size is as same as the ferrite strip on the top surface.

Figure 3.16: Alumina substrate with a ferrite strip on the top surface

After the ion mill etching, 1 um Platinum layer is deposited on the substrate. To avoid Platinum coating on the sidewalls, tape is used during Platinum coating. As a result, the microstrip line is a little shorter than the simulation. The final device is shown in figure 3.17.

Figure 3.17: 60GHz isolator

3.6 Results and Discussion

In chapter 2, it was shown that the return loss of the 60GHz device with test platform is under -20dB, and the insertion loss is also reasonable. The same test jig was used for the SIW isolator test.

3.6.1 60GHz Test Setup

The 60GHz SIW isolator with taper transitions and microstrip lines is inserted into the hole inside the test platform, and copper tape is used to connect the SIW to the isolator. A 7700Oe magnet (KJ-D4X0DIA-N52, K&J magnet Inc.) was used as the magnet bias. Figure 3.18 is a picture of the 60GHz H-plane resonance isolator based on SIW with magnet bias in the test platform. The measurements were performed in a R&S ZVA 67GHz vector network analyzer (Rohde & Schwarz Inc.).

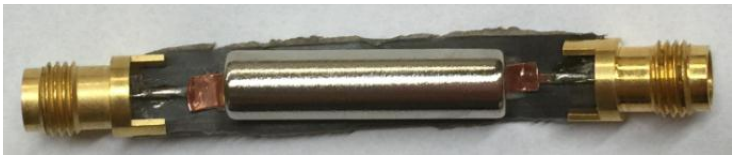

Figure 3.18: 60GHz SIW isolator with test platform and magnet bias

3.6.2 Isolator with Single-side Ferrite Strip

The isolation of 60GHz with 300nm thick single ferrite strip is shown in figure 3.19 after the test platform and microstrip-taper-SIW insertion losses have been removed. The maximum isolation occurs at 58.3GHz, which is close to 60GHz. The isolation is about -8dB.

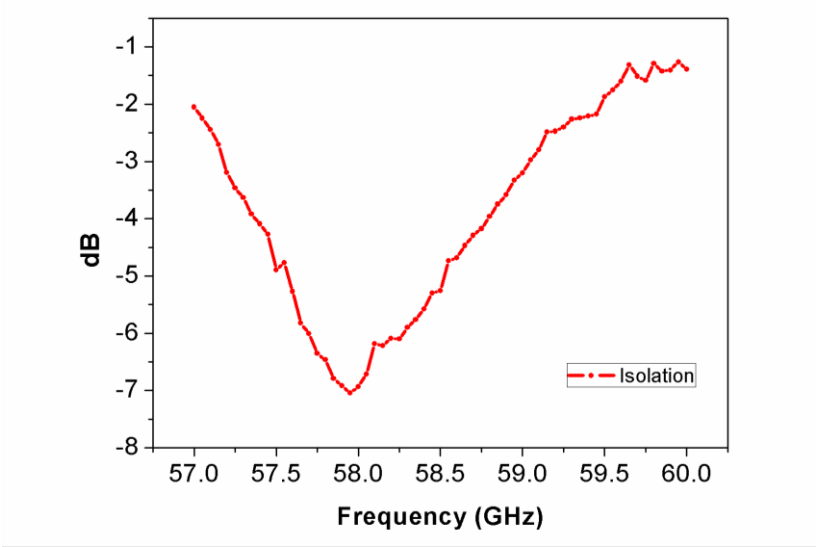

Figure 3.19: Isolation of 60GHz isolator with single side ferrite strip

3.6.3 Isolator with Double-side Ferrite Strip

The second isolator has double-side ferrite strips. The total thickness of the ferrite layers is 600nm. Figure 3.20 shows that the isolation can achieve -11dB at 58.3GHz. The difference between the two isolators is caused by the different space ratio. The space ration of the single-side ferrite is about 0.0003, while for double-side ferrite strip, this value is 0.0006. With a larger space ratio, a better isolation may be achieved.

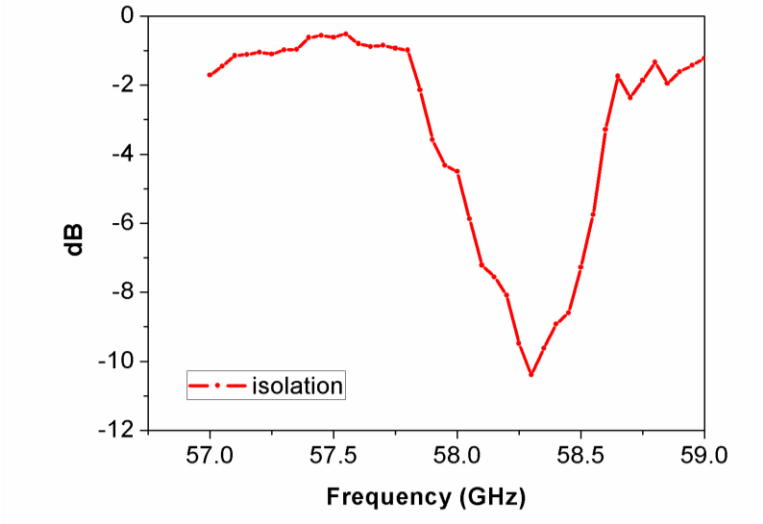

Figure 3.20: Isolation of 60GHz isolator with double-side ferrite strips

The difference between the two isolators is caused by the different space ratio. With a larger space ratio, a better isolation may achieve. Besides, the performance of H-plane isolator is related to the location of the ferrite strip. The previous ferrite location calculation assumes the ferrite thickness is 500nm. And the total thickness of double-side ferrite strip is 600nm, which is closer to the simulation compares to the single side ferrite strip (300 nm).

The isolator has its maximum isolation at 58GHz because the magnet bias used in the test is 7700 Oe instead of 8100 Oe. Theoretically by increasing the magnetic bias, the working frequency can be modified to 60GHz.

3.7 60GHz Microstripline Isolator

The aboved esults are based on SIW. To compare different planar isolators, a 60GHz microstripline isolator is designed. The sketch of the isolator is shown in figure 3.21.

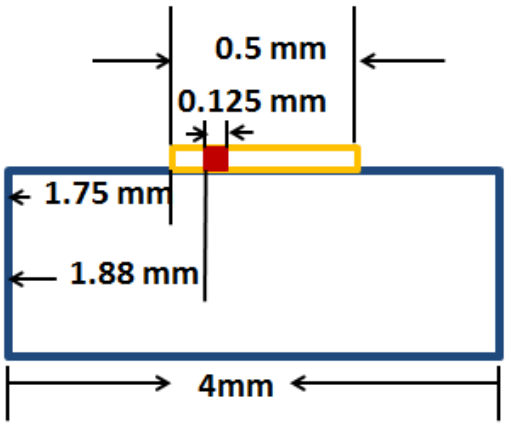

Figure 3.21: The sketch of 60GHz microstripline isolator

The isolator is simulated by HFSS. The length is set to be 5mm. The simulation results are shown in figure 3.22.

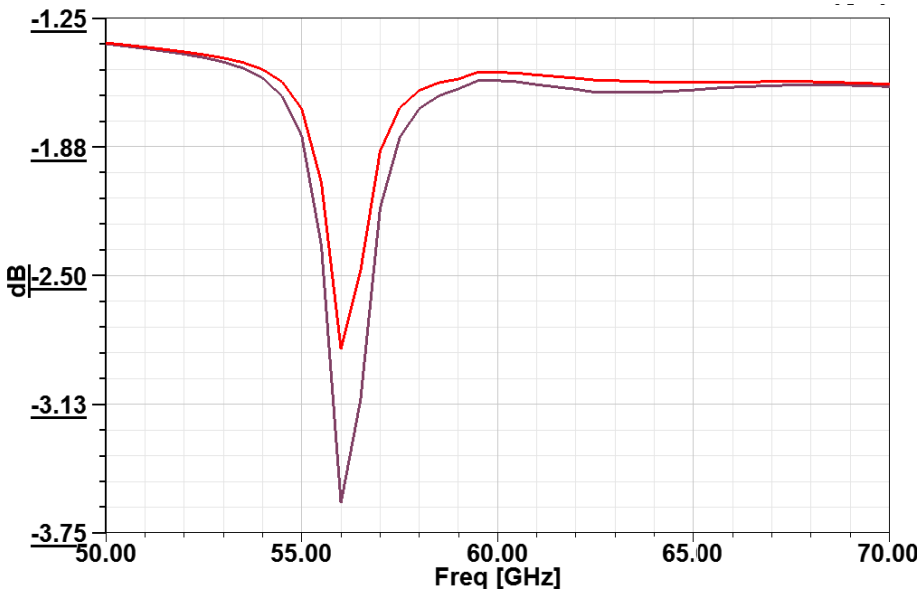

Figure 3.22: Simulation result of 60GHz microstripline isolator

From the simulation results, it is found that microstripline isolator has a smaller insertion loss (1dB/cm) compared to the SIW (2dB/cm). However, the isolation of microstripline isolator is much smaller (1dB/cm) than the isolation of H-plane resonance isolator (4dB/cm). As a result, H-plane resonance isolator will be discussed in the next chapter.

CHAPTER 4

THE 60GHZ TUNABLE ISOLATOR

4.1 The Magnetoelectric Effect Coupling of Multiferroic Heterostructures

Magnetoelectric effect (ME) coupling is caused by the cross interaction between two or more ferroic materials, the magnetic or electric properties can be changed by applying an external electric or magnetic filed. Multiferroic heterostructures combine two or more ferroic materials together. Reports found that the magnetic property and the electronic properties are coupled in the multiferroic heterostructures, which caused a strong ME coupling inside the heterostructure. So it is possible to control the magnetic property of the multiferroic heterostructure by applying an external electric field [89-91].

The first type of the multiferroic heterostructure is the ferromagnetic-ferroelectric-layered heterostructure [92-93]. This structure combines a ferromagnetic thin film together with ferroelectric thin film. For this kind of material, an application of DC voltage bias will cause a change of dielectric constant of ferroelectric layer, and this dielectric constant change will bring a change of frequency in the hybrid magnetoelectric mode, therefore the FMR frequency of the ferromagnetic layer will change [94].

The second type is the ferromagnetic–piezoelectric-layered-heterostructures [95-96]. This structure is composed by ferromagnetic thin film and piezoelectric thin film. For this heterostructure, the stress of the piezoelectric layer will be changed with a DC voltage bias; and then a stress change will also result in the ferromagnetic layer, which leads to a change of magnetic property and a FMR frequency shift [97-98].

Based on the thin film heterostructures, it is possible to make ferrite devices with electric tunability. Besides, the thin film property makes the device easy to realize on a planar structure especially for SIW. Compared to conventional tunable microwave magnetic devices, which are tuned by magnetic fields, the electronically tunable microwave multiferroic devices can be much more energy efficient, less noisy, compact, and lightweight [99].

4.2 Thin Film Ferromagnetic–ferroelectric-layered Heterostructure

In this project, the ferromagnetic-ferroelectric-layered heterostructure is used. Reports have been proved that the BaM/Pt/BST can produce a tunable FMR response at millimeter waveband with a small magnetic bias [33]. Here, a thin film BaM/Pt/BST heterostructure will be made and its magnetic performance will be measured.

4.2.1 Barium/Platinum/Barium Strontium Titanate (BST) Heterostructure

It is shown in the chapter 3 that BaM can produce a FMR response at millimeter waveband with a small magnetic bias. Moreover, ferroelectric-based $Ba_{1-x}Sr_xTiO_3$ (BST) has been widely used for microwave applications because its dielectric constant shows nonlinear variation with an applied electric field [100-102]. The bias field dependent dielectric constant makes it possible to make electrically tunable microwave devices. The advantages of using BST for tunable microwave applications are its low loss, large tunability, and adjustable Curie temperature through the choice of chemical composition [103-104]. Some RF devices have been realized by this method [105-107]. Combining

BaM and BST together, it is possible to make a tunable ferrite device working at millimeter wave band with a small magnetic bias.

Besides, reports show that to help combine the BaM layer and the BST layer, a Pt layer is needed [32-34]. Using this method, the 60GHz planar isolator can be electrically tunable.

4.2.2 Fabrication Processes

The BaM coating used the same define (CSD) process in chapter 3. A 500nm thick BaM layer is deposited on the alumina substrate first. Then a 50nm thick Pt layer is deposited on top of the BaM layer. The Pt layer plays an important role in the oriented growth of BST layer [33], it provides a good template for epitaxial BST growth so that the mismatch between BaM layer and BST layer can be reduced to the lowest level.

The BST layer is also deposited on the Pt layer by CSD process. The optimized BST precursor solution for dip-coating is prepared by dissolving Barium and strontium acetates in D. I. water and 2 methoxyethanol (2MOE). The ratio of H2O to 2MOE is 1:4. A small amount of acetic acid is added as stabilizer. Then stoichiometric amount of Titanium (diisopropoxide) bis(2,4-pentanedionate) (TIAA), 75% in isopropanol, is added into the solution. The concentration of the precursor solution is 0.02M. Using this method a high quality BST layer is successfully coated on the substrate. This dip coating was performed by Dr. X. Guo of Boston Technology Inc., Woburn, MA.

The SEM picture of the BaM/Pt/BST heterostructure is shown in figure 4.1.

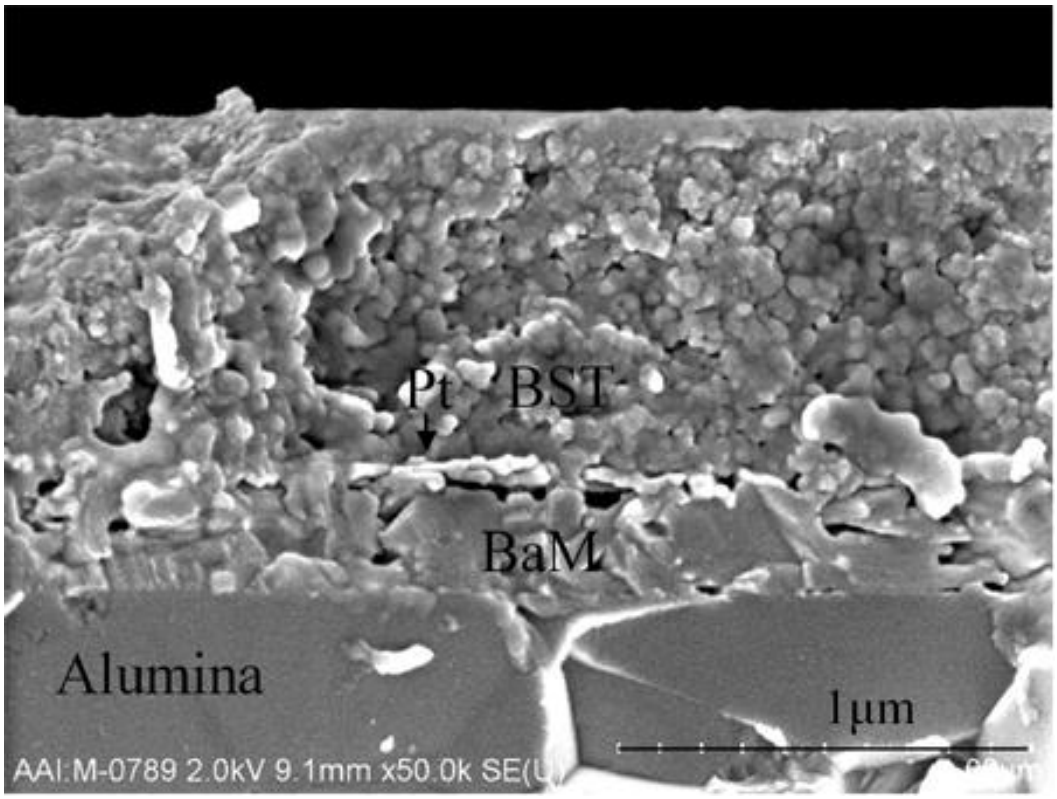

Figure 4.1: A BST/Pt/BaM/alumina heterostructure

4.2.3 Electric Tuning Characterization

To get the electric tuning characterization of the ferromagnetic-ferroelectric-layered heterostructure, first the electric hysteresis loop of BST is measured using an alumina substrate with BaM/Pt/BST coating. The electric hysteresis loop shows how the polarization (P) changes with the external electric field (E). The P-E loop in figure 4.2 implies that the BST layer works functionally and the high polarization value is caused by the high permittivity of the material.

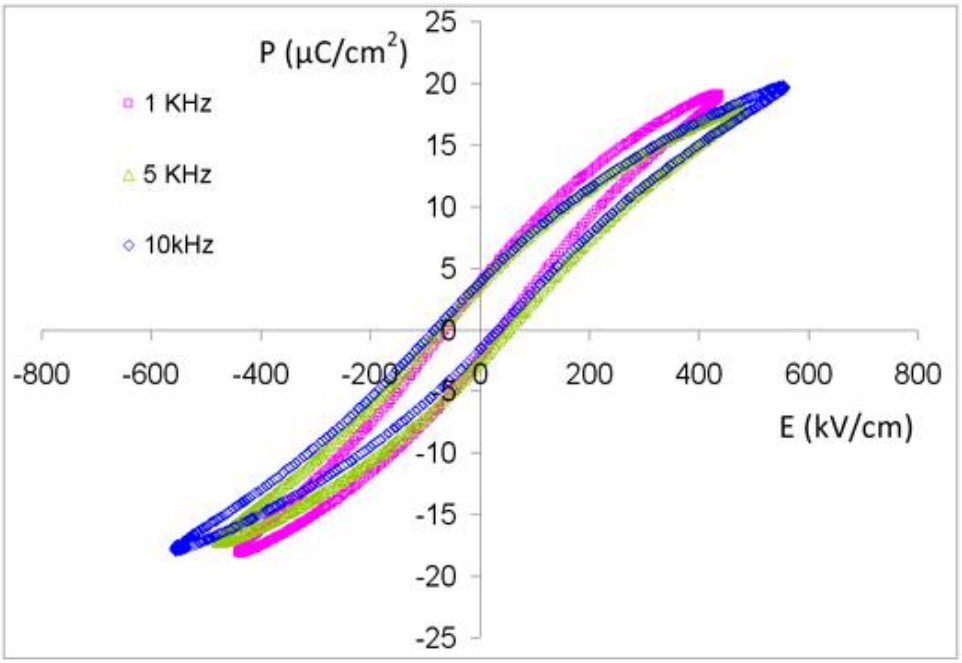

Figure 4.2: P-E loop of BST on alumina substrate with BaM/Pt/BST coating

To get the electric tuning characterization of the ferromagnetic-ferroelectric-layered heterostructure, the dielectric properties of the BaM/Pt/BST layer on alumina substrate are measured using an SR720 LCR Meter (Stanford Research System) and an XHR 150-7 DC Power Supply (Xantrex). Test results in figure 4.3 shows that the sample shows tunability with the DC voltage bias change, and the electric tunability of the structure can be as high as 2.1MHz/V.

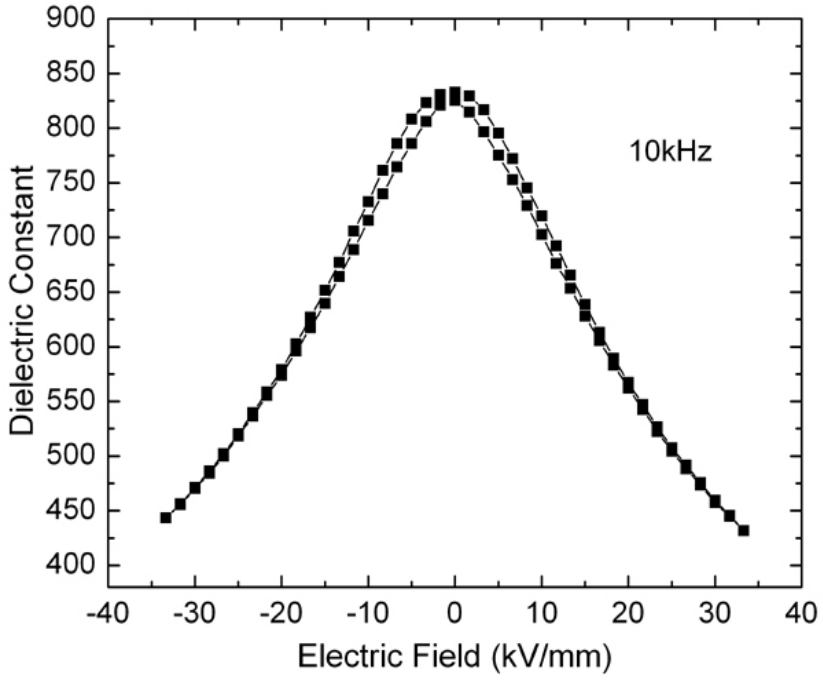
Dielectric Constant
Electric Field (kV/mm)
10kHz
900
850
800
750
700
650
600
550
500
450
400
-40
-30
-20
-10
0
10
20
30
40

(a)

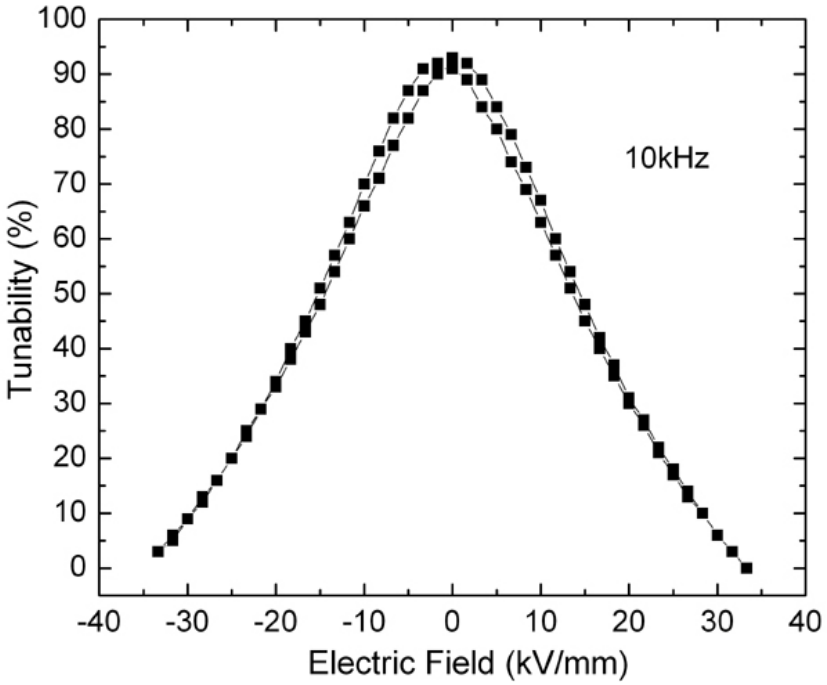
Tunability (%)
Electric Field (kV/mm)
10kHz
100
90
80
70
60
50
40
30
20
10
0
-40
-30
-20
-10
0
10
20
30
40

(b)

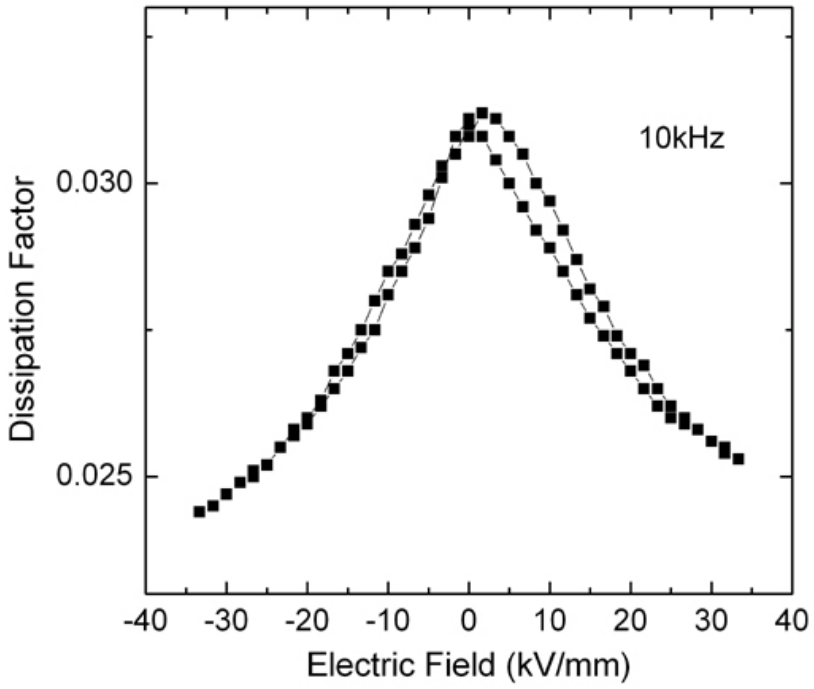

(c)

Figure 4.3: Dielectric properties of BaM/Pt/BST varies with electric field: (a) dielectric constant; (b) tunability; (c). dissipation factor

4.3 Voltage Biased Tunable Isolator

Based on the results in chapter 2 and chapter 3, to make a tunable 60GHz isolator based on SIW, a 0.25mm thick alumina substrate is used. And to reduce the loss at high frequency, Platinum is used as the conducting layer. The sketch of the device is shown in figure 4.3. On top of the 60GHz SIW, first a BaM thin film will be deposited. After that, a Pt layer will be coated. On top of the Pt layer, there is a BST layer. Finally, the Pt electrode will be patterned on the BaM/Pt/BST heterostructure.

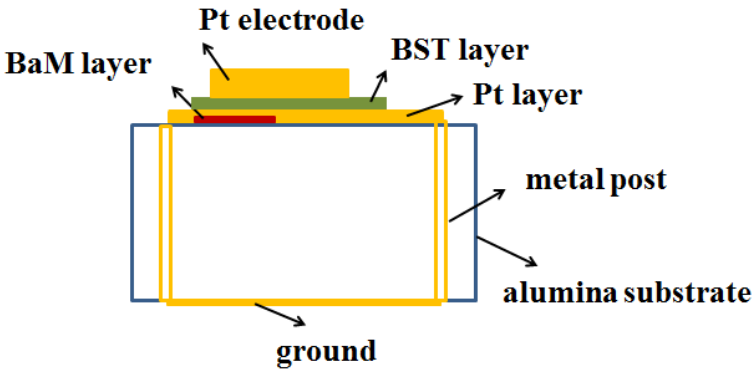

Figure 4.4: 60GHz tunable H- isolator based on SIW with BaM/Pt/BST layers

4.4 Fabrication

The isolator is built on a 60GHz SIW with microstrip lines and taper transitions. A 0.25mm thick alumina sheet is used as the substrate. To meet on the 10dB isolation requirement, the length the SIW is set to be 21mm. The whole structure is fabricated on a 26mm*4mm rectangular alumina substrate. And the holes of SIW are drilled on the substrate by laser drilling.

The 60GHz tunable isolator based on SIW is fabricated by MEMS technologies. Figure 4.4 shows the fabrication of the tunable isolator. To metalize the holes, firstly a Platinum layer is sputtered inside the holes array. To avoid the skin depth effect [48], the thickness of the Platinum layer should be larger than 660nm, so the thickness of the sputtered Platinum is 1um. After the sputter, a 300nm thick BaM thin film is deposited on top of the substrate by CSD process. The BaM layer is then etched into strip by ion mill. After the patterning, a 50nm thick Platinum layer is sputtered on the ferrite strip to develop the connect layer between BaM and BST. The other area is coated by a 1 um

thick Platinum layer as the conducting layer of SIW. A BST layer is deposited on top of the Platinum layer, and it is patterned by ion mill. Finally, the electrode, the microstrip lines and the taper transitions are built by a lift off process.

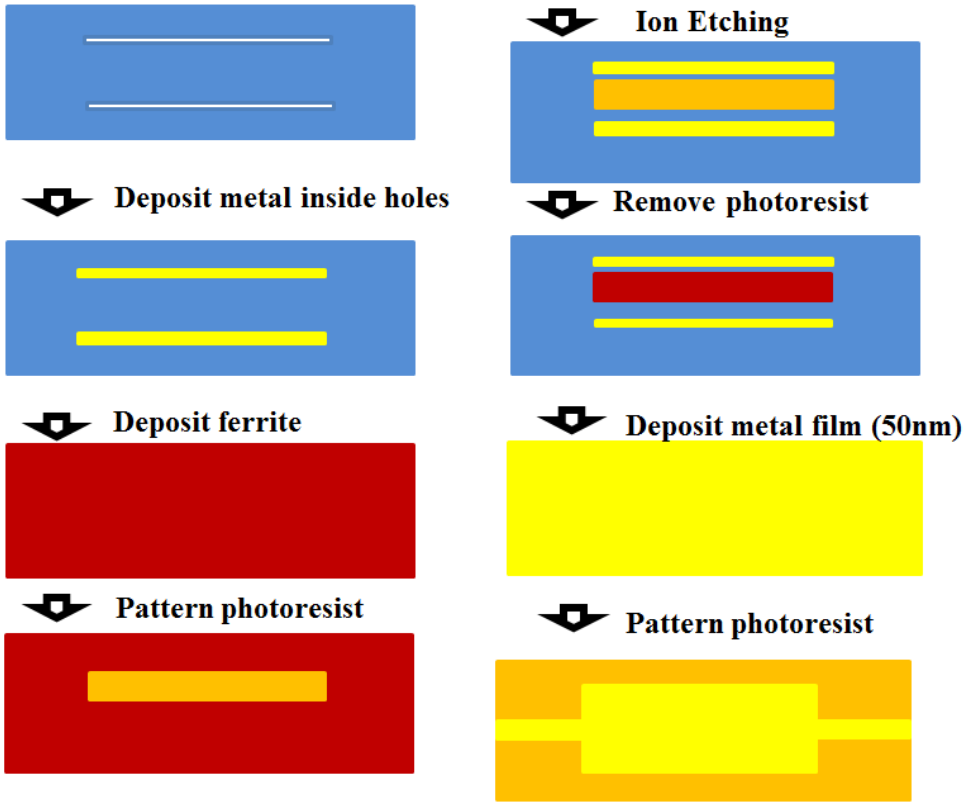

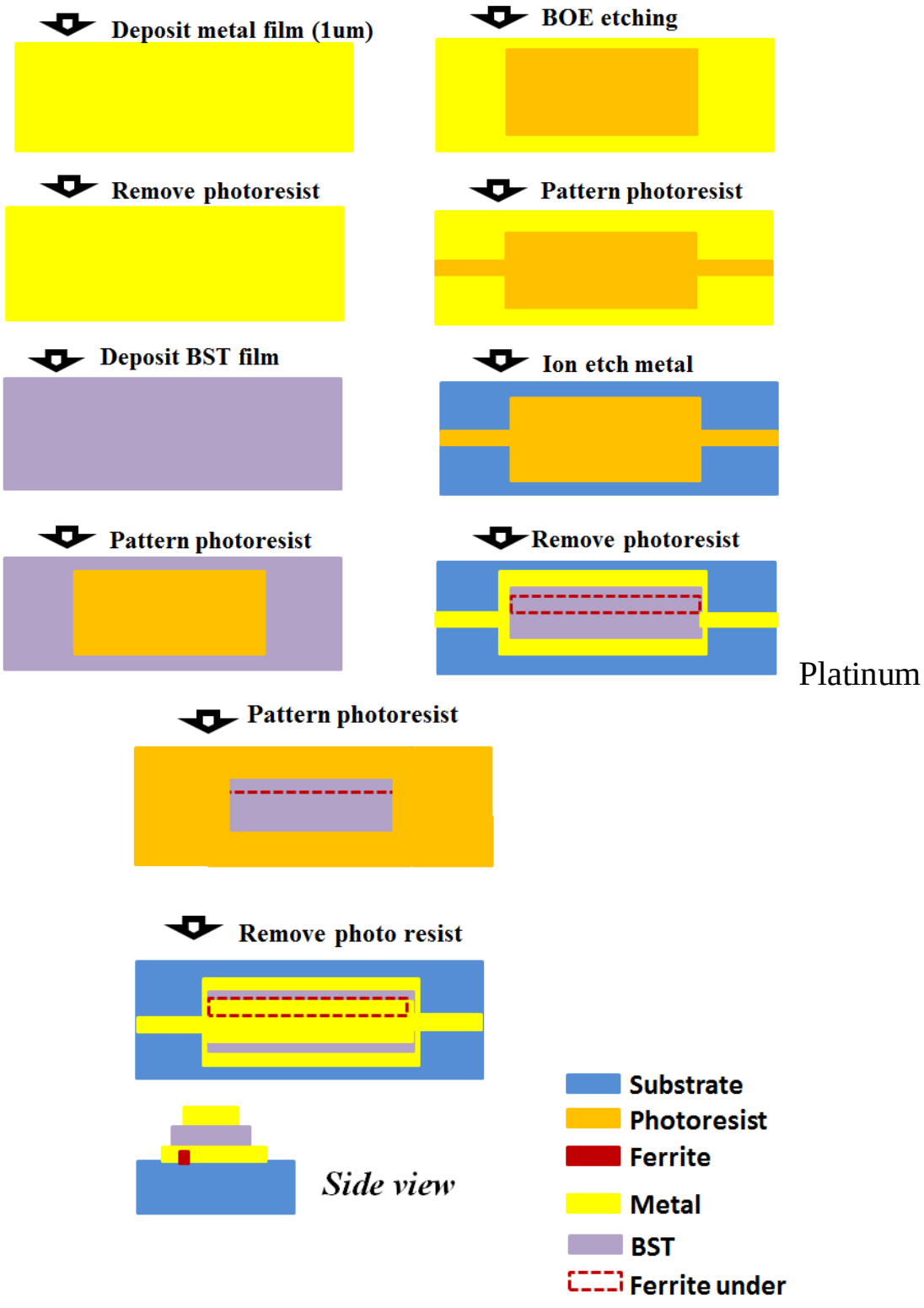

Figure 4.5: Fabrication process of 60GHz tunable isolator based on SIW

The final device is shown in figure 4.5 (a), a detailed look of the tunable isolator is shown in figure 4.5 (b). As are shown in the figures, the device fabrication is done successfully. The ferrite strip is underneath the bottom Platinum layer, and the BST layer is coated on top of the 50nm thick bottom Platinum layer. The top Platinum layer is served as the electrode for the test.

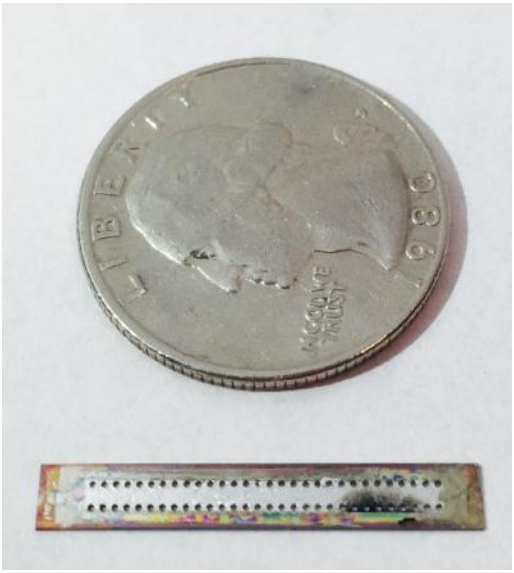

(a)

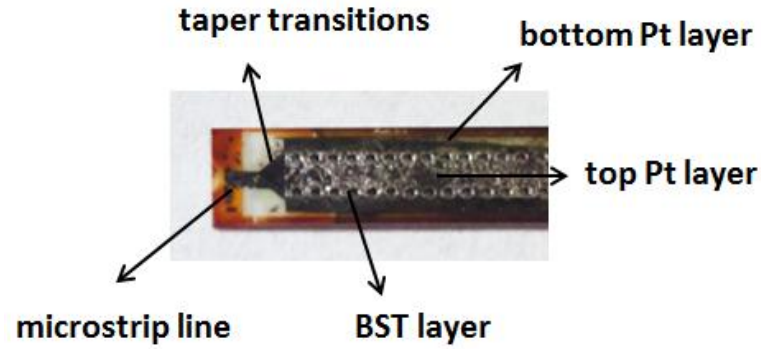

(b)

Figure 4.6: (a) BaM ferrite strip on 60GHz SIW; (b) 60GHz H-plane resonance isolator based on SIW

4.5 Results and Discussion

The performance of the 60GHz tunable isolator based on the SIW is measured. Since the size of the 60GHz device is small, it will be difficult to measure the performance directly. As a result, the isolator is connected to the outside equipment through a test platform. The test platform with the 60GHz tunable isolator is shown in figure 4.6 (a). The test platform has a hole inside of it so that the isolator can be installed. The 60GHz microstrip lines on the test platform connect the isolator to the 1.85mm connectors. The test platform is built on a Rogers RT5880 substrate. The magnetic bias is a 7700Oe permanent magnet (KJ-D4X0DIA-N52, K&J magnet Inc.). Figure 4.5 (b) shows the 60GHz tunable isolator based on SIW with magnet bias in test platform.

(a)

(b)

Figure 4.7: (a) 60GHz test platform; (b) 60GHz tunable isolator based on SIW with test platform and permanent magnet

The performance of 60GHz H-plane isolator is measured by R&S ZVA vector network analyzer (Rohde & Schwarz Inc.). Since the insertion loss could not be measured directly, table 1 shows the insertion loss of the 60GHz tunable isolator with and without test platform. According to the test result, the insertion loss of the 60GHz isolator based on SIW is about -4dB.

The performance of the tunable isolator with different voltage bias is shown in figure 4.7. The same structure for the isolator in chapter 3 operates at 57GHz instead of 60GHz because of the 7700 Oe magnet. The 60GHz tunable isolator measurement result shows that the isolation point changes with the voltage. Without any bias, the isolation point is at 57.32 GHz, the isolation is about 13.01dB. With a 10V bias, the isolation point moves to 57.305GHz, and the isolation changes to 12.85dB. By increasing the voltage to 20V, the isolation point decreased to 57.295GHz, and the isolation is 12.44dB.

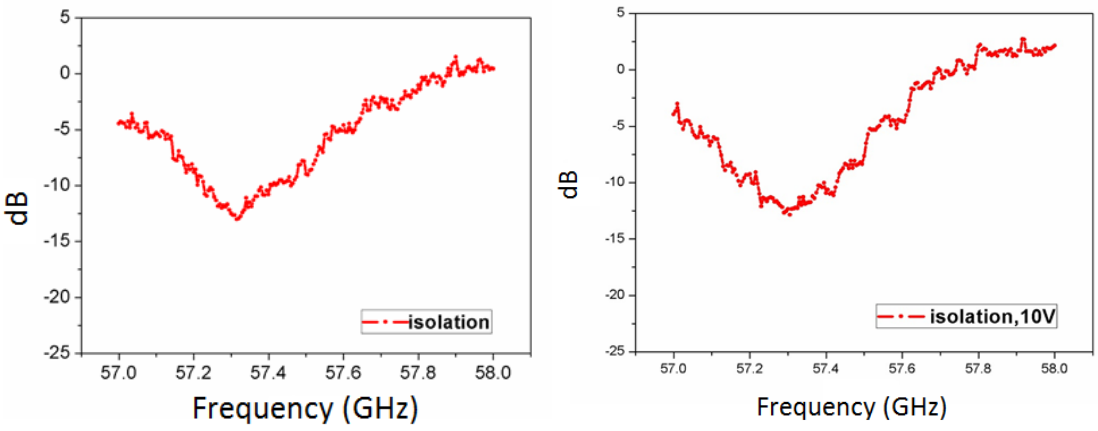

(a) (b)

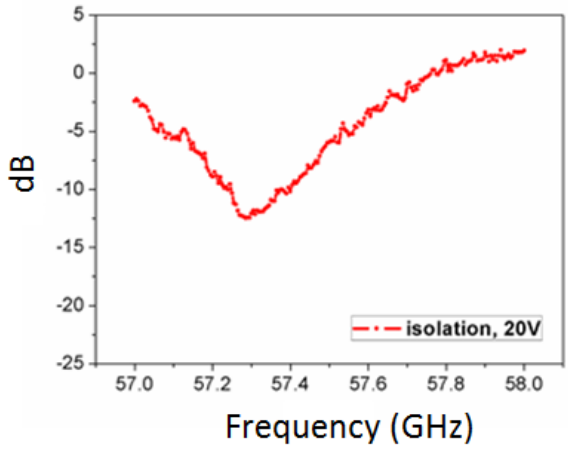

(c)

Figure 4.8: Test results on 60GHz tunable isolator with (a) no DC bias; (b) 10V DC bias; (c) 20V DC bias

From the test results, it can be seen that the isolator works functionally at 57GHz with a 7700Oe magnetic bias, and the isolation is about 13dB. Besides, the frequency moves with the voltage changes. The tuning rate of the device is about 1MHz/V. As same as the 60GHz H-plane resonance isolator in chapter 3, if the magnetic bias can be increased to 8000Oe, the working frequency will be increased to 60GHz. The results also prove that the BaM/Pt/BST heterostructure shows an electronic tunability at high frequency, which allows the design of ferrite tunable devices possible for wide bandwidth structures.

CHAPTER 5

Conclusions

5.1 Summary

The main objective of the project is to develop a planar isolator working at 60GHz. Using SIW technology, a 60GHz device with high performance and low cost can be realized, also the planar structure makes it easy to be integrated into a subsystem. The traditional planar isolator usually works under V band due to the low FMR frequencies. The appearance of thin film BaM ferrite makes it possible to realize a FMR frequency at the millimeter waveband, which allows the isolator working at 60GHz. Based on this structure, a voltage biased isolator is realized. This tunable isolator employs the multiferroic thin film heterostructure so that the dielectric constant of the device can be controlled by the DC voltage bias.

In chapter 2, first a model of 60GHz SIW on alumina substrate with Platinum coating was designed. Two types of SIW are simulated by HFSS, the single post rows and the double post rows Although the simulation results show that SIW with double-layer-post rows has a better performance, due to the fabrication limit, SIW with single-layer-post rows is used. 60GHz microstrip lines and taper transitions are designed to connect SIW with 1.85mm connectors. The SIW with different taper transition lengths are compared, simulation results suggest that $3\lambda/4$ long taper transition can give the smallest insertion loss. 60GHz SIW is fabricated by nanofabrication technologies, and the posts are machined by laser drilling. A 60GHz test platform is developed to run the measurement, because at high frequency the component size is too small to solder the connectors. The

insertion loss and the return loss are measured by 60GHz vector network analyzer, results show that the insertion loss of the SIW is -4dB and the return loss is under -20dB in the working band.

Based on the results in chapter 2, a 60GHz isolator was developed in chapter 3. The principle of ferrite device is first introduced. After that, a C-axis thin film BaM ferrite is employed to realize self-bias property at 60GHz. VSM measurement shows that the thin film BaM ferrite has a high anisotropic field compared to the traditional bulk single crystal BaM. Besides, FMR linewidth is very narrow (around 110 Oe) from 58GHz to 63GHz with a small DC magnetic bias. Three types of ferrite isolator are simulated and compared based on the magnetic properties of thin film BaM. Results show that H-plane resonance isolator has the best performance. The optimized ferrite strip position is calculated by Matlab to get the maximum isolation. Two types of H-plane resonance isolator are fabricated. One has only one ferrite strip on top side, while the other one has ferrite strips on both sides. A 7700 Oe magnet is used for the DC magnetic bias during the test. Results show that the isolation of the single-side ferrite strip is -8dB while the double-side ferrite strip achieves -11 dB. Both of the isolators operate at 58GHz because of the lower magnetic bias.

A voltage biased tunable isolator was realized in chapter 4. The electric tuning property of multiferroic thin film heterostructures is first described. Then BaM/Pt/BST heterostructure is introduced, experiment results show that this type of heterostructure shows an electric tunability as high as 2.1MHz/V at 58GHz frequency. A tunable isolator with BaM/Pt/BST is designed; the structure is as same as the 60GHz self-biased isolator

with single-side ferrite strip except that the coating layer is BaM/Pt/BST other than BaM. The device is built and measured at 57 GHz, it shows an electric tunability around 1MHz/V.

5.2 Conclusions

It was proved in this thesis that SIW is a promising structure for 60GHz communication subsystems. Since the 60GHz SIW shows a low loss at the millimeter waveband, it can be used for ferrite devices with high performance at high frequency. The thin film BaM ferrite shows a narrow FMR linewidth and high anisotropic magnetic field at 60GHz, which makes it a good choice for making ferrite devices at the millimeter waveband. A H-plane resonance isolator with BaM thin film is realized and works functionally at 58GHz. Even though a 7700 Oe permanent magnet is used, the whole system is compact and low cost compared to the other isolators. Working at such a high frequency a bulky and expensive electromagnet needs to be employed to make ferrite device work, the permanent magnet choice is the better option. Based on the magnetic properties of BaM, a BaM/Pt/BST multiferroic thin film heterostructures was developed. Since the dielectric constant of BST can be modified with voltage bias, the whole structure shows an electric tunability at high frequency. The results prove that the 60GHz isolator with BaM/Pt/BST can be controlled by a DC voltage bias together with a DC magnetic bias. With the voltage bias changes, the working frequency of the maximum isolation point changes. The planar structure as well as the of ferrite isolator based on SIW provide an opportunity to integrate the components into the 60GHz tiny chip-set communication subsystem with high performance and low cost.

5.3 Future Suggestions

First, other transmission lines can be used for 60GHz ferrite devices. Although SIW shows a low insertion loss during the test, other types of waveguides such as coplanar waveguide is also an alternative at millimeter waveband [145]. Besides, using these transmission lines may avoid taper transitions, which add insertion loss to the system.

Second, the magnetic properties of BaM can be improved by using buffering layer between BaM coating layer and the substrate [146-147]. Since the performance of the ferrite device depends on the ferrite material, the buffer layer will help the adhesion of the ferrite layer on the substrate, which will in turn decrease the defects of the ferrite layer. In this way, the DC magnetic bias needed for measurement may be decreased so that the ferrite device can work at 60GHz with a smaller magnet or even without magnet.

Third, there are two types of multi-thin film heterostructures for electric tuning, but only ferromagnetic-ferroelectric heterostructure was studied. Several reports proved that the ferroelectric-piezoelectric heterostructure can be used on RF components [148-150]. BST/PZT is such a heterostructure, and it has shown electric tunability at high frequency and can also be used for voltage biased ferrite isolator [151]. Using this type of heterostructure together with BaM can help the ferrite device work functionally at 60GHz just as the ferrite isolator developed in chapter 4, and the performance of these two isolators can be compared.

Reference

[1] S. Yong and C. Chong, An Overview of Multigigabit Wireless through Millimeter Wave Technology: Potentials and Technical Challenges, EURASIP Journal on Wireless Communications and Networking, VOL. 2007, Article ID 78907.
[2] ITU-R, Radio Regulations, Edition of 2012.
[3] S. Roy, J. Foerster, V. Somayazulu, and D. Leeper, Ultrawideband Radio Design: The Promise of High-Speed, Short-Range Wireless Connectivity, Proceedings of the IEEE, VOL. 92, NO. 2, February 2004.
[4] FCC, First Report and Order, FCC 02-48.
[5] M. Peter, W. Keusgen, J.Luo, A Survey on 60 GHz Broadband Communication: Capability, Applications and System Design, Proceedings of the 3rd European Microwave Integrated Circuits Conference, 978-2-87487-007-1, 2008.
[6] N. Guo, R. Qiu, S. Mo and K. Takahashi, 60-GHz Millimeter-Wave Radio: Principle, Technology, and New Results, EURASIP Journal on Wireless Communications and Networking., pp. 1-8, 2007.
[7] C. Park, T. Rappaport, Short-Range Wireless Communications For Next-Generation Networks: Uwb, 60 Ghz Millimeter-Wave Wpan, and Zigbee, IEEE Wireless Communications., Vol. 14, Iss. 4, pp. 70-78, Aug. 2007.
[8] L. Yang, 60GHz: Opportunity for Gigabit WPAN and WLAN Convergence, in ACM SIG COMM Computer Communication Review, New York, NY, 2009, Vol. 39, NO.1 , pp. 56-61
[9] H. Liebe, P. Rosenkranz, G. Hufford, Atmospheric 60-GHz oxygen spectrum: New laboratory measurements and line parameters, doi:10.1016/0022-4073(92)90127-P
[10] P. Smulders, 60GHz: Exploiting the 60 GHz Band for Local Wireless Multimedia Access: Prospects and Future Directions, IEEE Communications Magazine, January 2002.
[11] M. Bozzi, A. Georgiadis, K. Wu, Review of substrate-integrated waveguide circuits and antennas, IET Microw. Antennas Propag., Vol. 5, Iss. 8, pp. 909–920, 2011.
[12] F. Shigeki, Waveguide line, Japan Patent 06-053 711, Feb. 25, 1994.
[13] D. Finley, R. Lewis, Microstrip lines and Slotlines. Boston, MA: Artech House, 2013, pp.497-498.
[14] D. Finley, R. Lewis, Printed circuit board, US Patent 4221925 A, Sep 1980.
[15] M. Gongora-Rubioa, P. Espinoza-Vallejosb, L. Sola-Lagunac, J. Santiago-Avilésb, Overview of low temperature co-fired ceramics tape technology for meso-system technology (MsST), doi:10.1016/S0924-4247(00)00554-9
[16] K. Samanta, D. Stephens, I. Robertson, 60 GHz multi-chip-module receiver with substrate integrated waveguide antenna and filter, Electronics Letters, Vol. 42, NO.12,pp. 701-702, Jun. 2006.
[17] F. Mira, J. Mateu, M. Bozzi, Substrate integrated waveguide predistorted filter at 20 GHz, IET Microw. Antennas Propag, Vol. 5, Iss.8, pp. 928-933, 2011.
[18] L. Yan, W. Hong, G. Hua, J. Chen, K. Wu, and T. Cui, Simulation and Experiment on SIW Slot Array Antennas, Ieee Microwave and Wireless Components Letters, Vol. 14, No. 9, September 2004

[19] Z. Li, K. Wu, 24-GHz Frequency-Modulation Continuous-Wave Radar Front-End System-on-Substrate, Ieee Transactions on Microwave Theory and Techniques, VOL. 56, NO. 2, FEB 2008.
[20] B. Floyd, S. Reynolds, U. Pfeiffer, A Silicon 60-GHz Receiver and Transmitter Chipset for Broadband Communications, IEEE Journal of Solid-State Circuits, Vol. 41, NO. 12, pp. 2820-2831, Dec. 2006.
[21] D. Pozar: Microwave Engineering. Hoboken, NJ: Wiley, 2012, pp.475-476.
[22] F. Fesharaki, C. Akyel, K. Wu, Broadband substrate integrated waveguide edge-guided mode isolator, Electronics Letters, Vol. 49, Iss. 4, pp. 269-271, 2013.
[23] V. Kerckhoven, L. Piraux, I. Huynen, Substrate integrated waveguide isolator based on ferromagnetic nanowires in porous alumina template, Appl. Phys. Lett., 105, 183107, 2014.
[24] Y. Cheng, Q. Huang, Y. Wang, Narrowband Substrate Integrated Waveguide Isolators, IEEE Microwave and Wireless Components Letters., Vol. 24, NO.10, pp. 698-700, Oct. 2014.
[25] Y. Fetisov, C. Patton, V. Synogach, Nonlinear Ferromagnetic Resonance and Foldover in Yttrium Iron Garnet Thin Films—Inadequacy of the Classical Model, IEEE Transactions on Magnetics, VOL. 35, NO. 6, NOV 1999
[26] W. Parys, D. Thourhout, R. Baets, B. Dagens, J. Decobert, O. Gouezigou, D. Make, and L. Lagae, Amplifying Waveguide Optical Isolator with an Integrated Electromagnet, IEEE Photonics Technology Letters, VOL. 19, NO. 24, DEC 15, 2007
[27] O. Zahwe, B. Abdel Samad, B. Sauviac, J. P. Chatelon, M. F. Blanc Mignon and J. J. Rousseau, YIG Thin Film Used To Miniaturize a Coplanar Junction Circulator, J. of Electromagn. Waves and Appl., Vol. 24, 25–32, 2010
[28] Y. Song, J. Das, P. Krivosik, H. Seo, M. Wu, Electric Tuning of Ferromagnetic Resonances in Hexagonal-Barium-Ferrite/Barium-Strontium-Titanate Heterostructures, IEEE Magnetics Letters, Vol. 1,Aug. 2010.
[29] S. Toncich, "Tunable Isolator," U.S. Patent 7 265 243 B2, Sep. 4, 2007
[30] S. Subbiah and A. Alphones: "Tunable isolator using a coupled microstrip line with an obliquely magnetised YIG substrate", IEE Proc.-Microw. Antennas Propag., Vol. 150, No. 4, Aug. 2003.
[31] J. Wu , M. Li , X. Yang , S. Beguhn , and N. Sun, A Novel Tunable Planar Isolator with Serrated Microstrip Structure, IEEE Transactions On Magnetics, Vol. 48, No. 11, Nov. 2012.
[32] Y. Song, J. Das, P. Krivosik, N. Mo, C. Patton, Electric field tunable 60 GHz ferromagnetic resonance response in barium ferrite barium strontium titanate multiferroic heterostructures, Applied Physics Letters., Vol. 1,Aug. 2010.
[33] J. Das, Y. Song, M. Wu, Electric-field control of ferromagnetic resonance in monolithic BaFe12O19–$Ba_{0.5}Sr_{0.5}TiO_3$ heterostructures, Journal Of Applied Physic,s vol. 94, 182505, 2009.
[34] T. M. Shaw, Z. Suoa, M. Huang, E. Liniger, R. B. Laibowitz, J. D. Baniecki, The effect of stress on the dielectric properties of barium strontium titanate thin films, Applied Physics Letters, Volume 75, Number 14, OCT 1999

[35] R. Heindl, H. Srikanth, S. Witanachchi1, P. Mukherjee1, T. Weller, A. S. Tatarenko and G. Srinivasan, Structure, magnetism, and tunable microwave properties of pulsed laser deposition grown barium ferrite/barium strontium titanate bilayer films, J. Appl. Phys. 101, 09M503, 2007
[36] A. A. Semenov, S. F. Karmanenko, V. E. Demidov, B. A. Kalinikos, G. Srinivasan, A. N. Slavin, J. V. Mantese, Ferrite-ferroelectric layered structures for electrically and magnetically tunable microwave resonators, Appl. Phys. Lett. 88, 033503, 2006
[37] S. Srinath, N. A. Frey, R. Heindl, H. Srikanth, K. R. Coffey, N. J. Dudney, Growth and characterization of sputtered BSTO⁄BaM multilayers, J. Appl. Phys. 97, 10J115, 2005
[38] F.Xu, K.Wu, Guided-Wave and Leakage Characteristics of Substrate Integrated Waveguide, IEEE Transactions on Microwave Theory and Techniques, VOL. 53, NO. 1, JAN 2005
[39] P. G. Li , A. T. Adams , Y. Leviatan and J. Perini "Multiple-post inductive obstacles in rectangular waveguide", IEEE Trans. Microw. Theory Tech, vol. MTT-32, no. 4, pp.365 -373 1984
[40] Y. Cassivi, L. Perregrini, P. Arcioni, M. Bressan, K. Wu, G. Conciauro, Dispersion Characteristics of Substrate Integrated Rectangular Waveguide, IEEE Microwave and Wireless Components Letters, VOL. 12, NO. 9, SEP 2002
[41] F. Xu, K. Wu, Numerical Multimode Calibration Technique for Extraction of Complex Propagation Constants of Substrate Integrated Waveguide, Microwave Symposium Digest, 2004 IEEE MTT-S International.
[42] F. Xu, K. Wu, Domain decomposition FDTD algorithm combined with numerical TL calibration technique and its application in parameter extraction of substrate integrated circuits, IEEE Microwave Theory and Techniques Society, Volume:54 , Issue: 1, 2006
[43] M. Bozzi, L. Perregrini, K. Wu, Modeling of Conductor, Dielectric, and Radiation Losses in Substrate Integrated Waveguide by the Boundary Integral-Resonant Mode Expansion Method, IEEE Transactions On Microwave Theory and Techniques, VOL. 56, NO. 12, DECEMBER 2008
[44] Yan, L.; Hong, W.; Wu, K.; Cui, T.J., Investigations on the propagation characteristics of the substrate integrated waveguide based on the method of lines, Microwaves, Antennas and Propagation, IEE Proceedings, Volume: 152, Issue: 1, 2005
[45] D. Sievenpiper, L. Zhang, R. Broas, N. Alexopolous, E. Yablonovitch, High-Impedance Electromagnetic Surfaces with a Forbidden Frequency Band, IEEE Transactions on Microwave Theory and Techniques, VOL. 47, NO. 11, NOV 1999
[46] M. Bozzi, L. Perregrini, K. W, A novel technique for the direct determination of multimode equivalent circuit models for substrate integrated waveguide discontinuities, DOI: 10.1002/mmce.20360
[47] L. H. Weng, Y. C. Guo, X. W. Shi, X. Q. Chen, An Overview on Defected Ground Structure, Progress In Electromagnetics Research B, Vol. 7, 173–189, 2008
[48] F. Ulaby, U. Ravaioli, Fundamentals of Applied Electromagnetics. Upper Saddle River, NJ, Pearson, 2010.

[49] D. Deslandes, K. WU, Accurate Modeling, Wave Mechanisms, and Design Considerations of a Substrate Integrated Waveguide, IEEE Transactions on Microwave Theory and Techniques, VOL. 54, NO. 6, JUNE 2006
[50] K. Wu, D. Deslandes, The Substrate Integrated Circuits - A New Concept for High-Frequency Electronics and Optoelectronics, Microwave Review, 2003
[51] F. Xu, Y. Zhang, W. Hong, K. Wu, T. Cui, Finite-Difference Frequency-Domain Algorithm for Modeling Guided-Wave Properties of Substrate Integrated Waveguide, IEEE Transactions on Microwave Theory and Techniques, VOL. 51, NO. 11, NOV 2003
[52] Q. Lai, C. Fumeaux, W. Hong, R. Vahldieck, Characterization of the Propagation Properties of the Half-Mode Substrate Integrated Waveguide, IEEE Transactions on Microwave Theory and Techniques, 2009
[53] Y. Dong, T. Itoh, Composite Right/Left-Handed Substrate Integrated Waveguide and Half Mode Substrate Integrated Waveguide Leaky-Wave Structures, IEEE Transactions on Antennas and Propagation, VOL. 59, NO. 3, MAR 2011
[54] W. Hong, B. Liu, Y. Wang, Q.a Lai, H. Tang, X.Yin, Y.Dong, Yan Zhang, K. Wu, Half Mode Substrate Integrated Waveguide: A New Guided Wave Structure for Microwave and Millimeter Wave Application, Millimeter Waves Systems, 2006
[55] Y. Dong, T. Itoh, Composite Right/Left-Handed Substrate Integrated Waveguide and Half Mode Substrate Integrated Waveguide Leaky-Wave Structures, IEEE Transactions on Antennas and Propagation, VOL. 59, NO. 3, MAR 2011
[56] N. Grigoropoulos, B. Sanz-Izquierdo, P. Young, Substrate Integrated Folded Waveguides (SIFW) and Filters, IEEE Microwave and Wireless Components Letters, VOL. 15, NO. 12, DEC 2005
[57] R. Wang, L. Wu, and X. Zhou, Compact Folded Substrate Integrated Waveguide Cavities and Bandpass Filter, Progress In Electromagnetics Research, PIER 84, 135–147, 2008
[58] Z. Wang, S. Bu, Z. Luo, A substrate integrated folded waveguide (SIFW) H-plane band-pass filter with double H-plane septa based on LTCC, Ultrasonics, Ferroelectrics, and Frequency Control, IEEE Transactions on, On page(s): 560 - 563 Volume: 59, Issue: 3, March 2012
[59] W. Che, L. Geng; K. Deng; Chow, Y.L., Analysis and Experiments of Compact Folded Substrate-Integrated Waveguide, Microwave Theory and Techniques, IEEE Transactions on, On page(s): 88 - 93 Volume: 56, Issue: 1, Jan. 2008
[60] D. Deslandes, M. Bozzi, P. Arcioni, K. Wu, Substrate Integrated Slab Waveguide (SISW) for Wideband Microwave Applications, 2003 IEEE rvITT-S Digest
[61] P. Mondal, K. Wu, Single Mode Operation of Substrate Integrated Non-Radiative Dielectric Waveguide and an Excitation Scheme of Mode, Microwave and Wireless Components Letters, IEEE, on page(s): 418 - 420 Volume: 23, Issue: 8, Aug. 2013
[62] A. Belenguer, H. Esteban, V. Boria, Novel Empty Substrate Integrated Waveguide for High-Performance Microwave Integrated Circuits", Microwave Theory and Techniques, IEEE Transactions on, on page(s): 832 - 839 Volume: 62, Issue: 4, April 2014
[63] H. Wang, D. Fang, B. Zhang, W. Che, Dielectric Loaded Substrate Integrated Waveguide (SIW) –Plane Horn Antennas, IEEE Transactions on Antennas and

Propagation, VOL. 58, NO. 3, MARCH 2010
[64] M. Bozzi, S.A. Winkler, K. Wu, Broadband and Compact Ridge Substrate Integrated Waveguides, IET Microw. Antennas Propag., 2010, Vol. 4, Iss. 11, pp. 1965– 1973
[65] A. Mallahzadeh, S. Esfandiarpour, Wideband H-Plane Horn Antenna Based on Ridge Substrate Integrated Waveguide (RSIW), Antennas and Wireless Propagation Letters, IEEE, On page(s): 85 - 88 Volume: 11, 2012
[66] A. Farrall, P. Young, Rotated Half-Mode Substrate Integrated Waveguide, Antennas and Propagation Conference (LAPC), 2013 Loughborough, On page(s): 514 - 517
[67] T. Djerafi, H. Aubert, K. Wu, Ridge Substrate Integrated Waveguide (RSIW) Dual-Band Hybrid Ring Coupler, Microwave and Wireless Components Letters, IEEE, On page(s): 70 - 72 Volume: 22, Issue: 2, Feb. 2012
[68] A. Ali, H. El-Shaarawy, H. Aubert, Miniaturized Hybrid Ring Coupler Using Electromagnetic Bandgap Loaded Ridge Substrate Integrated Waveguide, Microwave and Wireless Components Letters, IEEE, on page(s): 471 - 473 Volume: 21, Issue: 9, Sept. 2011
[69] D. Pozar: Microwave Engineering. Hoboken, NJ: Wiley, 2012
[70] D. Deslandes, Design Equations for Tapered Microstrip-to-Substrate Integrated Waveguide Transitions, in IEEE MTT-S International Microwave Symposium Digest, Anaheim, CA, 2010, pp. 704-707.
[71] K. Lu, An Efficient Method for Analysis of Arbitrary Nonuniform Transmission Lines, IEEE Transactions on Microwave Theory and Techniques, VOL. 45, NO. 1, JAN 1997
[72] R. Hoffman, Handbook of Microwave Integrated Circuits, Artech House, Norwood, MA, 1983
[73] D. Linkhart, Microwave Circulator Design, Artech House, Norwood, MA, 1989
[74] A. Morrish,The Physical Principles of Magnetism, pp. 696. ISBN 0-7803-6029-X. Wiley-VCH , January 2001
[75] V. Harris, A. Geiler, Y. Chen, S. Yoon, M. Wu, A. Yang, Z. Chen, P. He, P. Parimi, X. Zuo, C. Patton, M. Abe, O. Acher, C. Vittoria, Recent advances in processing and applications of microwave ferrites, Journal of Magnetism and Magnetic Materials, 2009
[76] B. Bayard, B. Sauviac, D. Vincent, Ferrite Isolators, Wiley, 15 APR 2005, DOI: 10.1002/0471654507.eme113
[77] G. Day, D. Payne, A. Barlow, J. Ramskov-Hansen, Faraday rotation in coiled, monomode optical fibers: isolators, filters, and magnetic sensors, Optics Letters, Vol. 7, Issue 5, pp. 238-240, 1982, doi: 10.1364/OL.7.000238
[78] E. Schlomann, on the theory of the ferrite resonance isolator, Microwave Theory and Techniques, IRE Transactions on 8.2 (1960): 199-206.
[79] S. Oliver, P. Shi, N. McGruer, C. Vittoria, W. Hu, H. How, S. W. McKnight, P. M. Zavracky. Integrated self-biased hexaferrite microstrip circulators for millimeter-wavelength applications, Microwave Theory and Techniques, IEEE Transactions on 49, no. 2 (2001): 385-387.
[80] J. Truedson, K. McKinstry, P. Kabos, Carl. Patton, High-field effective linewidth and eddy current losses in moderate conductivity single-crystal M-type barium hexagonal ferrite disks at 10–60 GHz. Journal of applied physics 74, no. 4 (1993): 2705-2718.

[81] Y. Song, S. Kalarickal, and C. E. Patton, “Optimized pulsed laser deposited barium ferrite thin films with narrow ferromagnetic resonance linewidths,” J. Appl. Phys. 94, 5103 (2003).
[82] V. Harris, Growth of high quality low loss ferrite materials on SiC substrates for microwave and mm-wave device applications, 2008, (Navy Case 97,665), U.S. Patent 8,029,921, 2011.
[83] Y. Chen, A. Geiler, T. Sakai, S. Yoon, C. Vittoria, V. Harris, Microwave and magnetic properties of self-biased barium hexaferrite screen printed thick films, 2006.
[84] Y. Akaiwa, et. al: “An application of a hexagonal ferrite to a millimeter-wave Y circulator”, IEEE transactions on Magnetics., Vol. 10, NO.2, pp. 374-378, 1974.
[85] V. Kamberský, On the Landau-Lifshitz relaxation in ferromagnetic metals, Canadian Journal of Physics 48, no. 24 (1970): 2906-2911.
[86] Y. Fetisov, G. Srinivasan, Electric field tuning characteristics of a ferrite-piezoelectric microwave resonator, Applied physics letters 88, no. 14 (2006): 143503.
[87] C. Kittel: “Ferromagnetic resonance”, J. Phys. Radium, 12 (3), pp.291-302, 1951.
[88] Z. Chen, V. Harris, Ferrite film growth on semiconductor substrates towards microwave and millimeter wave integrated circuits, Journal of Applied Physics 112, no. 8 (2012): 081101.
[89] W. Eerenstein, N. Mathur, J. Scott, Multiferroic and magnetoelectric materials, nature 442, no. 7104 (2006): 759-765.
[90] C. Nan, M. Bichurin, S. Dong, D. Viehland, G. Srinivasan, Multiferroic magnetoelectric composites: historical perspective, status, and future directions, Journal of Applied Physics 103, no. 3 (2008): 031101.
[91] Y. Chu, L. Martin, M. Holcomb, M. Gajek, S. Han, Q. He, N. Balke, Electric-field control of local ferromagnetism using a magnetoelectric multiferroic, Nature materials 7, no. 6 (2008): 478-482.
[92] M. Bichurin, V. Petrov, G. Srinivasan, Theory of low-frequency magnetoelectric effects in ferromagnetic-ferroelectric layered composites, Journal of applied physics 92, no. 12 (2002): 7681-7683.
[93] H. Shigeki, H. Nishikawa, H. Nakai, J. Ishii, M. Nakamori, A. Fujimaki, Y. Noguchi, H. Tabata, T. Kawai, Preparation of all-oxide ferromagnetic/ferroelectric/superconducting heterostructures for advanced microwave applications, Superconductor Science and Technology 12, no. 11 (1999): 836.
[94] R. Ramaroorthy, and N. Spaldin, Multiferroics: progress and prospects in thin films, Nature materials 6, no. 1 (2007): 21-29.
[96] S. Spurgeon, J. Sloppy, D. Kepaptsoglou, P. Balachandran, S. Nejati, J. Karthik, A. Damodaran, Thickness-dependent crossover from charge-to strain-mediated magnetoelectric coupling in ferromagnetic/piezoelectric oxide heterostructures, ACS nano 8, no. 1 (2013): 894-903.
[96] G. Liu, Y. Zhang, P. Ci, S. Dong, Enhanced electrical manipulation of magnetic susceptibility in ferromagnetic amorphous alloy and piezoelectric bimorph heterostructure, Journal of Applied Physics 114, no. 6 (2013): 064107.

[97] S. Polisetty, W. Echtenkamp, K. Jones, X. He, S. Sahoo, C. Binek, Piezoelectric tuning of exchange bias in a $BaTiO_3$/Co/CoO heterostructure, Physical Review B 82, no. 13 (2010): 134419.
[98] D. Filippov, Theory of the magnetoelectric effect in ferromagnetic-piezoelectric heterostructures, Physics of the Solid State 47, no. 6 (2005): 1118-1121.
[99] S. Zygmunt, D. Bochenek, Multiferroic materials for sensors, transducers and memory devices (review article), Archives of Acoustics 33, no. 2 (2008): 243-260.
[100] P. Padmini, R. Taylor, M. Lefevre, A. Nagra, R. York, J. Speck, Realization of high tunability barium strontium titanate thin films by rf magnetron sputtering, Applied Physics Letters 75, no. 20 (1999): 3186.
[101] H. Li, A. Roytburd, S. Alpay, T. Tran, L. Salamanca-Riba, R. Ramesh, Dependence of dielectric properties on internal stresses in epitaxial barium strontium titanate thin films, Applied Physics Letters 78, no. 16 (2001): 2354-2356.
[102] Z. Ban, S. Alpay, Optimization of the tunability of barium strontium titanate films via epitaxial stresse, Journal of applied physics 93, no. 1 (2003): 504-511.
[103] A. Tombak, Jon-Paul Maria, F. Ayguavives, Z. Jin, G. Stauf, A. Kingon, A. Mortazawi , Tunable barium strontium titanate thin film capacitors for RF and microwave applications, Microwave and Wireless Components Letters, IEEE 12, no. 1 (2002): 3-5.
[104] W. Ma, L. Cross, Flexoelectric polarization of barium strontium titanate in the paraelectric state, Applied Physics Letters 81 (2002): 3440-3442.
[105] A. Tombak, Ali, J. Maria, F. Ayguavives, Z. Jin, G. Stauf, A. Kingon, A. Mortazawi, Voltage-controlled RF filters employing thin-film barium-strontium-titanate tunable capacitors, Microwave Theory and Techniques, IEEE Transactions on 51, no. 2 (2003): 462-467.
[106] N. Jayesh, D. Ghosh, J. Maria, A. Kingon, W. Fathelbab, P. Franzon, M. Steer, An electronically tunable microstrip bandpass filter using thin-film Barium-Strontium-Titanate (BST) varactors, Microwave Theory and Techniques, IEEE Transactions on 53, no. 9 (2005): 2707-2712.
[107] J. Sigman, C. Nordquist, P. Clem, G. Kraus, P. Finnegan, Voltage-controlled Ku-band and X-band tunable combline filters using barium-strontium-titanate, Microwave and Wireless Components Letters, IEEE 18, no. 9 (2008): 593-595.